RESULTS AND DISCUSSION

The analysis and interpretation of the various sections of the present work is as follows -

4.1 Selection of potential Antimicrobial peptide against *Staphylococcus aureus* toxins

4.1.1 The 3D structures of antimicrobial peptides

All the four selected antimicrobial peptides are of length less than or equal to 20 amino acids. All the structures of antimicrobial peptides predicted using Pepfold3 server are linear structures.

4.1.1.1 JCpep7

JCpep7 is a seven amino acid long peptide. It gives a linear structure as shown in the figure below.

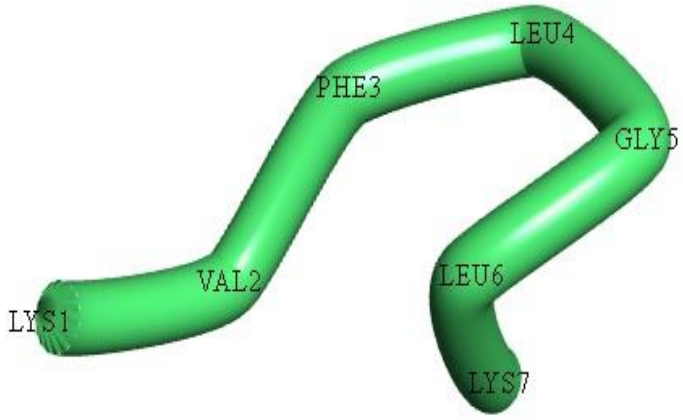

FIGURE 4.1: The figure shows the predicted structure of JCpep7, predicted using Pepfold3

4.1.1.2 Sesquin

Sesquin is a ten amino acid long peptide. It gives a linear structure as shown in the figure below.

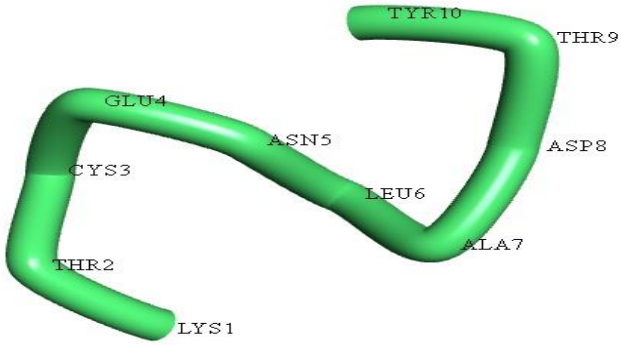

FIGURE 4.2: The figure shows the predicted structure of Sesquin, predicted using Pepfold3

4.1.1.3 Snakin-2

Snakin-2 is a fifteen amino acid long peptide. It gives a linear structure as shown in the figure below.

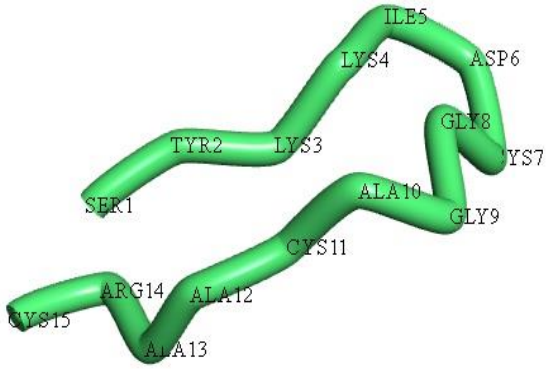

FIGURE 4.3: The figure shows the predicted structure of Snakin-2, predicted using Pepfold3

4.1.1.4 Ib-AMP1

Ib-AMP1 is a twenty amino acid long peptide. It gives a linear structure as shown in the figure below.

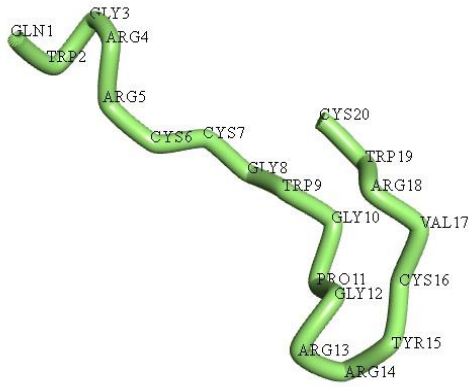

FIGURE 4.4: The figure shows the predicted structure of Ib-AMP1, predicted using Pepfold3

4.1.2 Docking results

The docking interaction studies were performed between the three toxins of *S. aureus*, i.e., ETA, ETB and PVL and the four antimicrobial peptides, i.e., JCpep7, Sesquin, Snakin-2 and Ib-AMP1. The best docked complexes of all the docking studies were analysed. The global energies and total non-bond interactions of all the sets of dockings are given below in the TABLE 4.1.

TABLE 4.1: The global energies, non-bond interactions and hydrogen bonds of the docked complexes of the toxins of *S. aureus* and antimicrobial peptides

Antimicrobial peptides	**Toxins of *Staphylococcus aureus***	**Global energy (kcal/mol)**	**Non - bond interactions**	**Hydrogen bond**
JCpep7	ETA	-21.22	11	1
	ETB	-18.28	10	2
	PVL	-7.80	5	0
Sesquin	ETA	-22.58	4	1
	ETB	-13.88	5	2

	PVL	-11.04	7	2
Snakin-2	ETA	-47.39	9	4
	ETB	-14.87	9	3
	PVL	-24.96	8	0
Ib-AMP1	ETA	-23.16	9	2
	ETB	-17.18	12	4
	PVL	-22.15	8	3

4.1.2.1 Docking of *S. aureus* toxins with JCpep7

The best docked complex of docking ETA with JCpep7 (shown in FIGURE 4.5) gave a global energy -21.22 kcal/mol. Total eleven non-bond interactions were formed between the residues of ETA and JCpep7 in this complex. Asp94, Asp34 and Asp37 residues of ETA

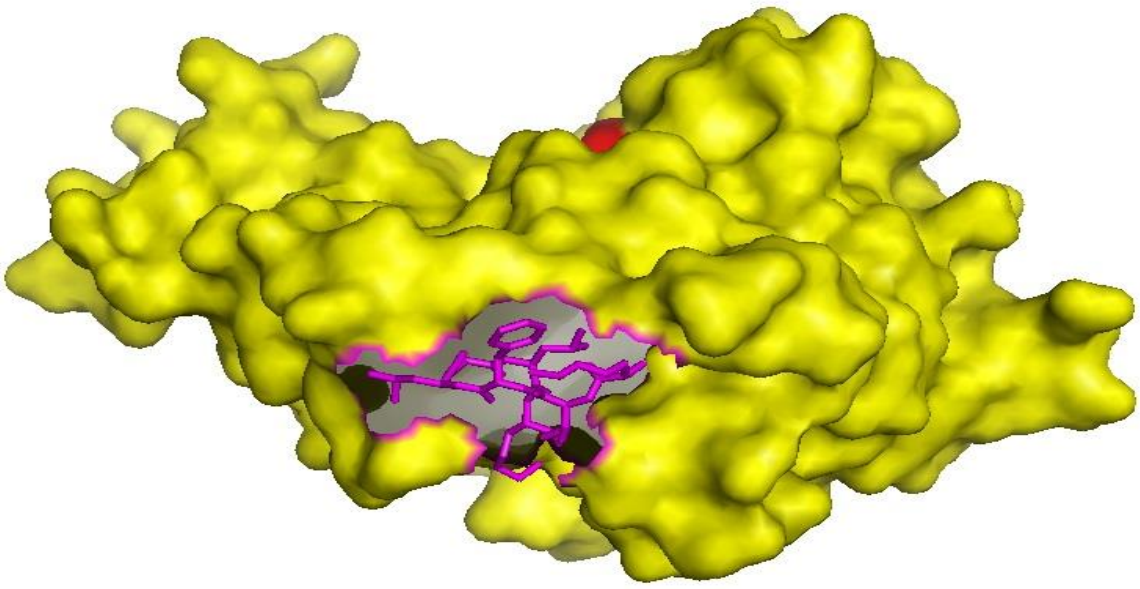

FIGURE 4.5: The figure shows best docked structure of ETA and JCpep7. The residues of ETA are shown in yellow colour and the residues of JCpep7 are shown in magenta. The red coloured residues show the crucial residues of ETA.

form electrostatic interactions with Lys1, Lys7 and Lys7 residues of JCpep7 respectively. One hydrogen bond is formed between Lys32 of ETA and Lys7 of JCpep7. His171 and Phe30 residues of ETA interact with Gly5 residue of JCpep7 to form carbon hydrogen bond. Lys27 residue of ETA forms two alkyl bonds with Leu4 and Lys7 residues of JCpep7. Lys32 and Lys166 residues of ETA form alkyl bonds with Leu6 residue of JCpep7. His171 residue of ETA form pi-alkyl bond with Leu6 residue of JCpep7.

The best docking interactions between ETB and JCpep7 were shown by the docked complex (shown in FIGURE 4.6) which had global energy -18.28 kcal/mol. Total ten non-bond interactions were formed between residues of ETB and JCpep7 in this complex. Glu196 and Asp143 of residues of ETB form Electrostatic interactions with Lys1 of JCpep7. Leu193 residue of ETB forms two hydrogen bonds with Lys7 of JCpep7. His141 and Lys149 residues of ETB form carbon hydrogen bonds with Lys1 and Lys7 residues respectively of JCpep7. Pro139, Leu193 and Lys194 residues of ETB form alkyl non-bond interactions with Lys1 and Leu6 residues respectively of JCpep7.

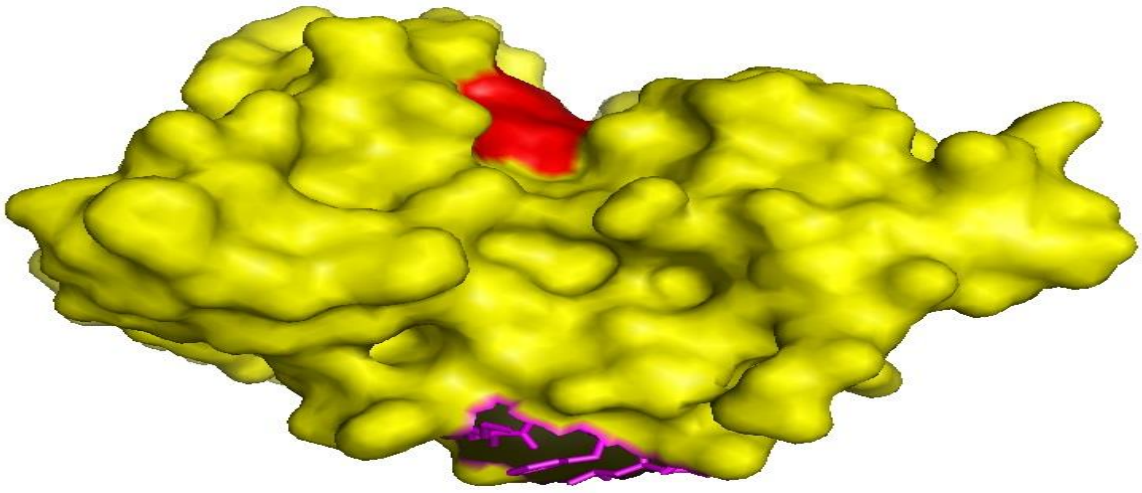

FIGURE 4.6: The figure shows best docked structure of ETB and JCpep7. The residues of ETB are shown in yellow colour and the residues of JCpep7 are shown in magenta. The red coloured residues show the crucial residues of ETB.

The best docking interactions between PVL and JCpep7 were shown by the docked complex (shown in FIGURE 4.7) which had global energy -7.80 kcal/mol. Total five non-bond interactions were formed between residues of PVL and JCpep7 in this complex. Lys212 residue of PVL forms electrostatic interaction with Lys7 residue of JCpep7. Trp176 residue of PVL forms two Pi-Alkyl interactions each with Lys1 and Val2 residues of JCpep7.

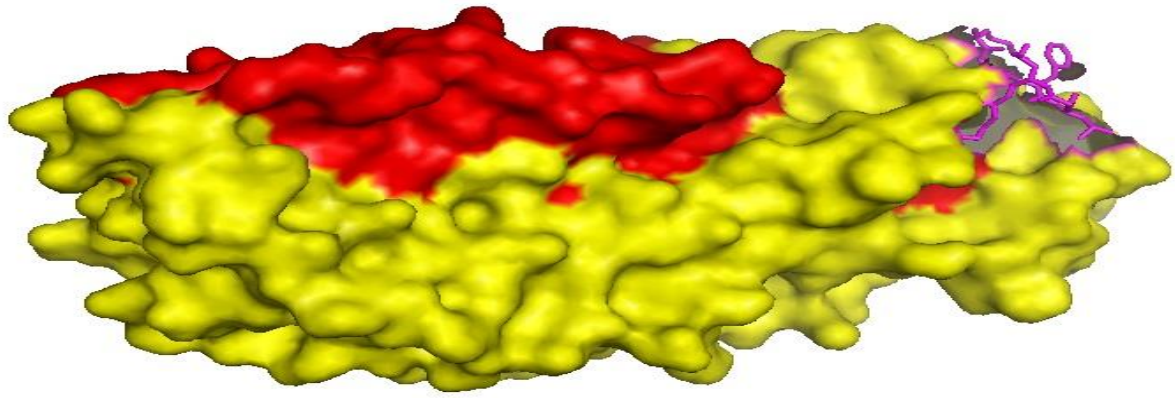

FIGURE 4.7: The figure shows best docked structure of PVL and JCpep7. The residues of PVL are shown in yellow colour and the residues of JCpep7 are shown in magenta. The red coloured residues show the crucial residues of PVL.

4.1.2.2 Docking of *S. aureus* toxins with Sesquin

The best docked complex of docking ETA with Sesquin (shown in FIGURE 4.8) gave a global energy -22.58 kcal/mol. Total four non-bond interactions were formed between the residues of ETA and Sesquin in this complex. Ser147 residue of ETA forms a hydrogen bond with Thr2 residue of Sesquin. Phe115 and Gly118 residues of ETA form carbon hydrogen bonds with Thr9 and Tyr10 residues respectively of Sesquin. Tyr232 residue of ETA forms a Pi-Alkyl interaction with Ala7 residue of Tyr10.

The best docked complex of docking ETB with Sesquin (shown in Figure 4.9) gave a global energy -13.88 kcal/mol. Total five non-bond interactions were formed between the residues

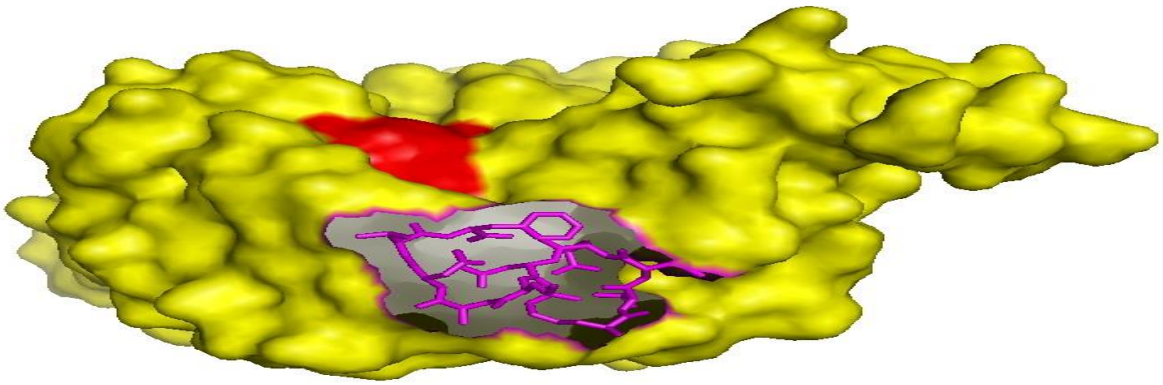

FIGURE 4.8: The figure shows best docked structure of ETA and Sesquin. The residues of ETA are shown in yellow colour and the residues of Sesquin are shown in magenta. The red coloured residues show the crucial residues of ETA.

of ETB and Sesquin in this complex. Glu23 residue of ETB forms a salt bridge with Lys1 residue of Sesquin. Arg33 residue of ETB forms electrostatic interaction with Asp8 residue of Sesquin. Arg33 and Gln166 residues of ETB form hydrogen bonds with Thr9 and Asp8 residues respectively of Sesquin. Leu193 forms Pi-Sigma interaction with Tyr10 residue of Sesquin.

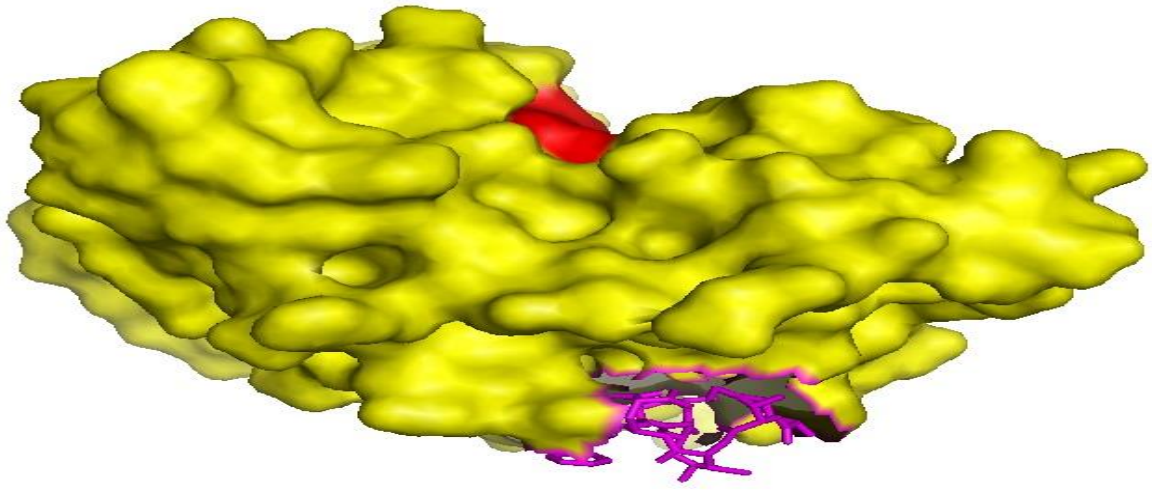

FIGURE 4.9: The figure shows best docked structure of ETB and Sesquin. The residues of ETB are shown in yellow colour and the residues of Sesquin are shown in magenta. The red coloured residues show the crucial residues of ETB.

The best docked complex of docking PVL with Sesquin (shown in FIGURE 4.10) gave a global energy -11.04 kcal/mol. Total seven non-bond interactions were formed between the residues of PVL and Sesquin in this complex. Lys295 and Asp89 residues of PVL form Electrostatic interaction with Tyr10 and Lys1 residues respectively of Sesquin. Thr242 and Asp291 residues of PVL form hydrogen bond with Lys1 and Cys3 residues respectively of Sesquin. Arg156 and Asp89 residues of PVL form carbon hydrogen bonds with Ala7 and Lys1 residues respectively of Sesquin. Ile277 residue of PVL forms Alkyl interaction with Cys3 residue of Sesquin.

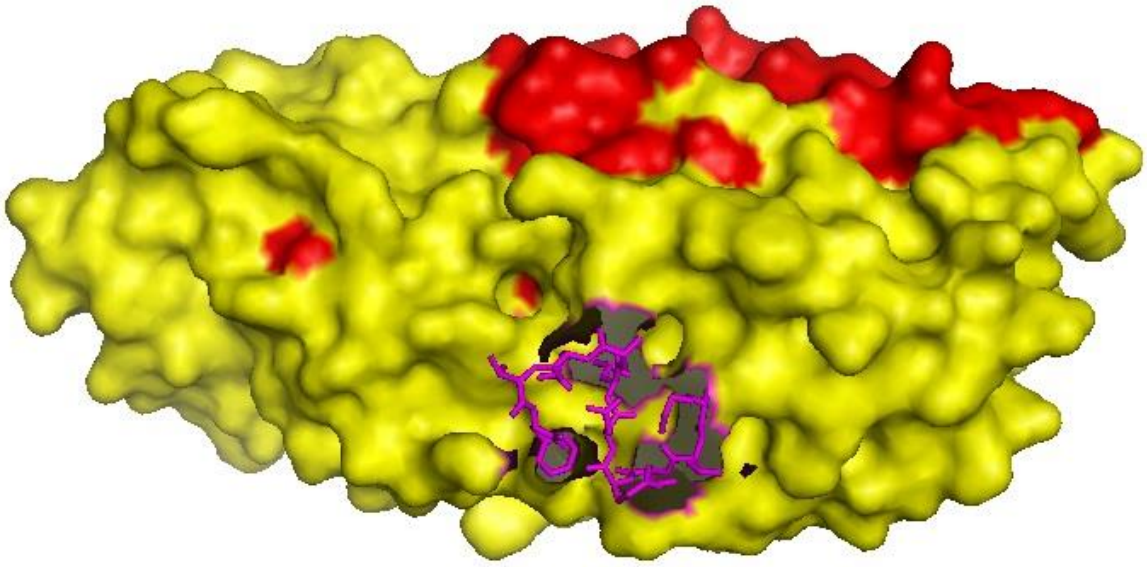

FIGURE 4.10: The figure shows best docked structure of PVL and Sesquin. The residues of PVL are shown in yellow colour and the residues of Sesquin are shown in magenta. The red coloured residues show the crucial residues of PVL.

4.1.2.3 Docking of *S. aureus* toxins with Snakin-2

The best docked complex of docking ETA with Snakin-2 (shown in FIGURE 4.11) gave a global energy -47.39 kcal/mol. Total nine non-bond interactions were formed between the residues of ETA and Snakin-2 in this complex. Arg219 residue of ETA forms two

electrostatic interactions with Asp6 residue of Snakin-2. Asn148, Arg182, Asn231 and Gly228 residues of ETA form hydrogen bonds with Cys15, Asp6, Cys15 and Ser1 residues respectively of Snakin-2. Gly118 residue of ETA forms Pi-Lone pair interaction with Tyr2 residue of Snakin-2. Arg182 and Val214 residues of ETA form Alkyl interactions with Lys3 and Ile5 residues respectively of Snakin-2.

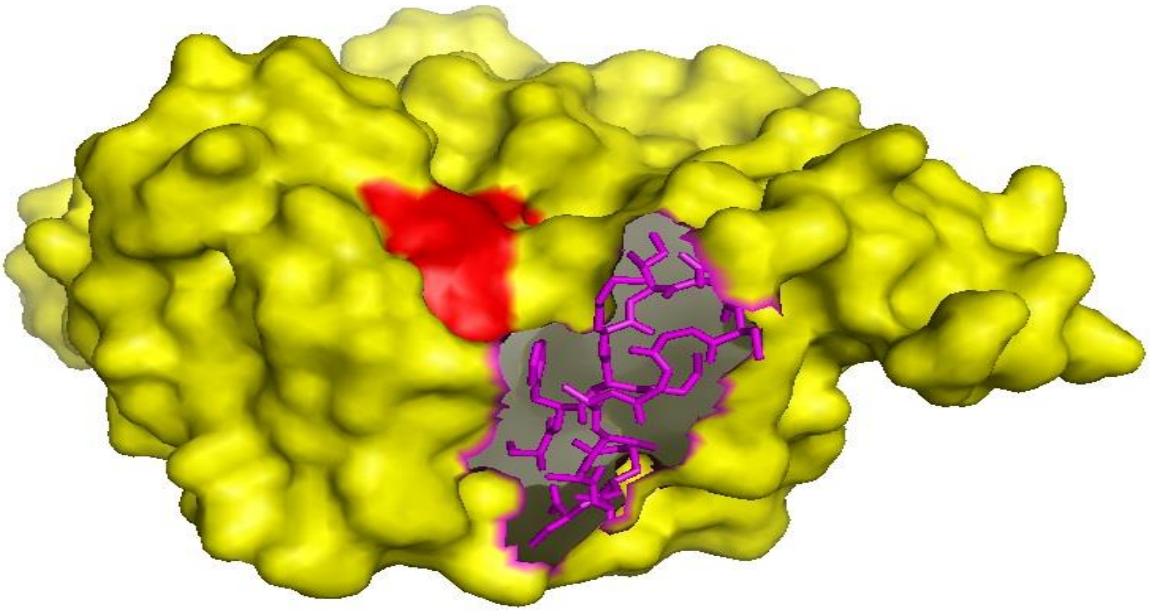

FIGURE 4.11: The figure shows best docked structure of ETA and Snakin-2. The residues of ETA are shown in yellow colour and the residues of Snakin-2 are shown in magenta. The red coloured residues show the crucial residues of ETA.

The best docked complex of docking ETB with Snakin-2 (shown in FIGURE 4.12) gave a global energy -14.87 kcal/mol. Total nine non-bond interactions were formed between the residues of ETB and Snakin-2 in this complex. Tyr150, Leu193 and His141 residues of ETB form hydrogen bonds with Gly9, Cys11 and Cys7 residues of Snakin-2. Leu193, Pro139 and Leu193 residues of ETB form Alkyl bond interaction with Lys3, Cys7 and Cys11 residues respectively of Snakin-2. Lys149 residue of ETB forms two alkyl bond interactions with

Ala12 and Ala13 residues of Snakin-2. Tyr150 residue of ETB forms Pi-Alkyl interaction with Cys11 residue of Snakin-2.

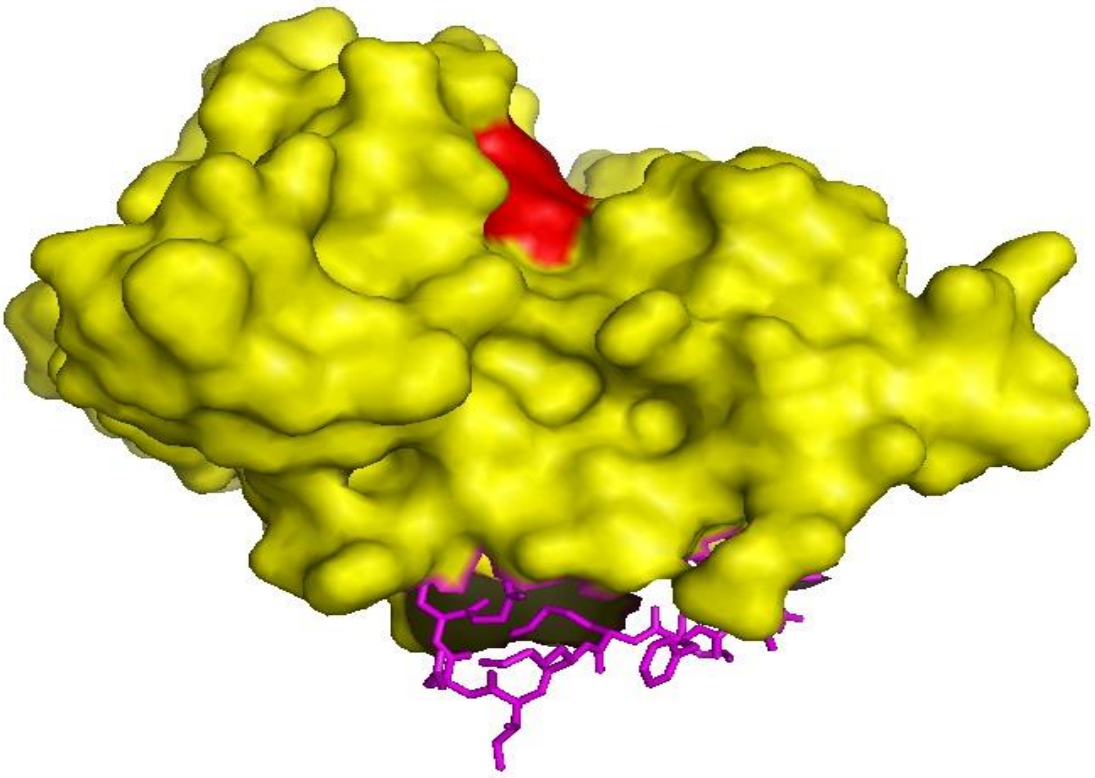

FIGURE 4.12: The figure shows best docked structure of ETB and Snakin-2. The residues of ETB are shown in yellow colour and the residues of Snakin-2 are shown in magenta. The red coloured residues show the crucial residues of ETB.

The best docked complex of docking PVL with Snakin-2 (shown in FIGURE 4.13) gave a global energy -24.96 kcal/mol. Total eight non-bond interactions were formed between the residues of PVL and Snakin-2 in this complex. Lys29 residue of PVL forms salt bridge with Cys15 residue of Snakin-2. Lys29 residue of PVL forms Carbon hydrogen bond with Arg14 residue of Snakin-2. His211 residue of PVL forms Pi-Sulfur bond with Cys7 residue of Snakin-2. Lys65 and Pro299 residue of PVL form Alkyl interaction with Cys11 and Cys15 residues of Snakin-2. Met300 residue of PVL forms two alkyl interactions with Ala13 and

Cys15 residues of Snakin-2. Tyr60 residue of PVL forms Pi-Alkyl interaction with Arg14 residue of Snakin-2.

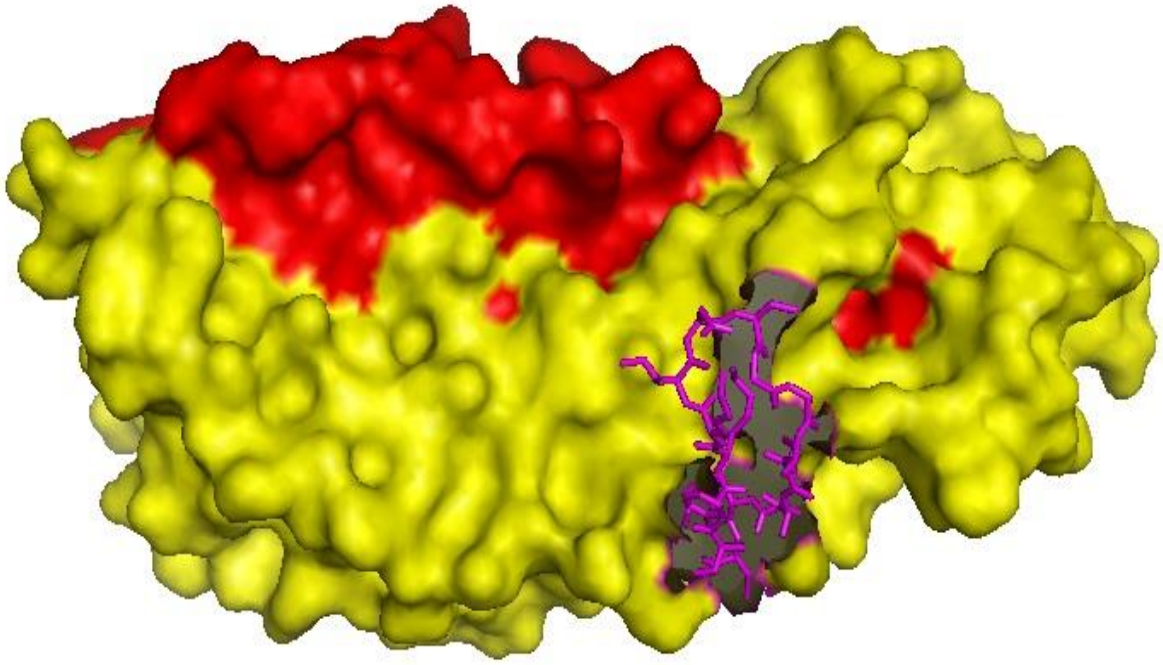

FIGURE 4.13: The figure shows best docked structure of PVL and Snakin-2. The residues of PVL are shown in yellow colour and the residues of Snakin-2 are shown in magenta. The red coloured residues show the crucial residues of PVL.

4.1.2.4 Docking of *S. aureus* toxins with Ib-AMP1

The best docked complex of docking ETA with Ib-AMP1 (shown in FIGURE 4.14) gave a global energy -23.16 kcal/mol. Total nine non-bond interactions were formed between the residues of ETA and Ib-AMP1 in this complex. His72 and Asp120 residues of ETA form hydrogen bonds with Gln1 residue of Ib-AMP1. His221, Ser212 and Glu11 residues of ETA form carbon hydrogen bond with Cys20, Arg4 and Arg18 residues respectively of Ib-AMP1. His 221 residue of ETA form Pi-Anion as well as Pi-Lone pair interaction with Cys20 of Ib-AMP1. Val 214 residue of ETA forms Alkyl interaction with Arg4 residue of Ib-AMP1. Arg14 residue of ETA forms Pi-Alkyl interaction with Arg18 residue of Ib-AMP1.

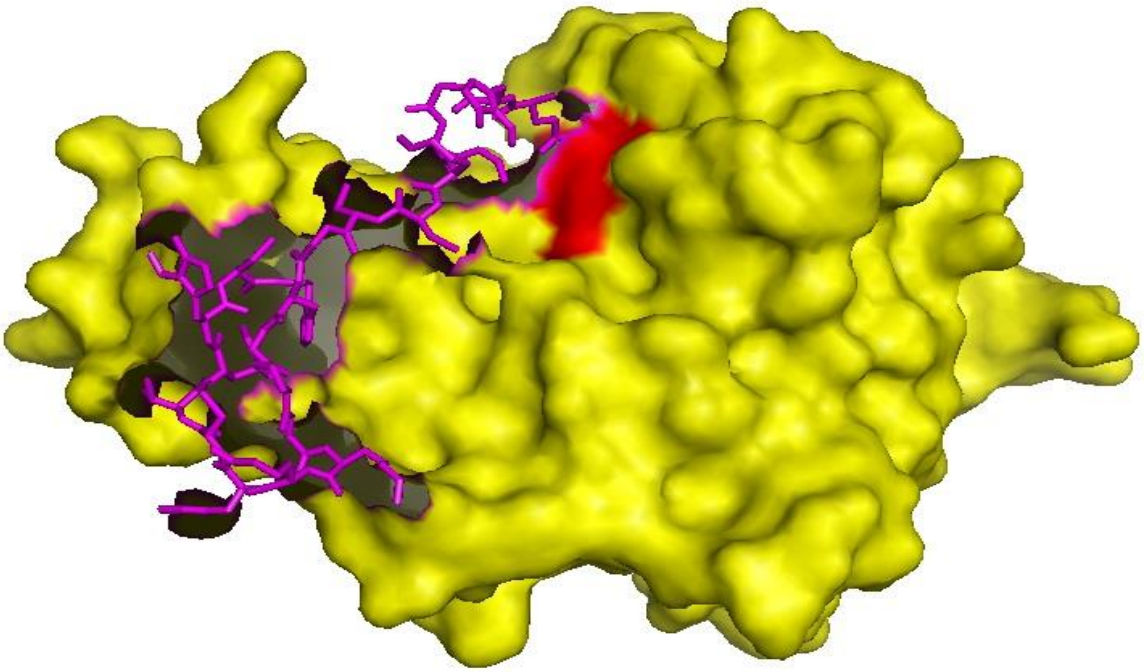

FIGURE 4.14: The figure shows best docked structure of ETA and Ib-AMP1. The residues of ETA are shown in yellow colour and the residues of Ib-AMP1 are shown in magenta. The red coloured residues show the crucial residues of ETA.

The best docked complex of docking ETB with Ib-AMP1 (shown in FIGURE 4.15) gave a global energy -17.18 kcal/mol. Total twelve non-bond interactions were formed between the residues of ETB and Ib-AMP1 in this complex. Lys204 and Asn173 residues of ETB form Hydrogen bond with Trp9 and Cys6 residues respectively of Ib-AMP1. Arg218 residue of ETB forms hydrogen bonds with Cys7 and Cys6 residues of Ib-AMP1. Gly203, Ser202 and Lys204 residues of ETB form carbon hydrogen bond with Trp9, Gly8 and Trp3 residues respectively of Ib-AMP1. Arg68 residue of ETB forms Pi-Cation interaction with Trp19 residue of Ib-AMP1. Lys204 residue of ETB forms Alkyl interaction with Pro11 and Arg13 residues of Ib-AMP1. Ile212 residue of ETB forms Alkyl interaction with Cys6 residue of Ib-AMP1. Arg218 residue of ETB forms Pi-Alkyl interaction with Trp2 residue of Ib-AMP1.

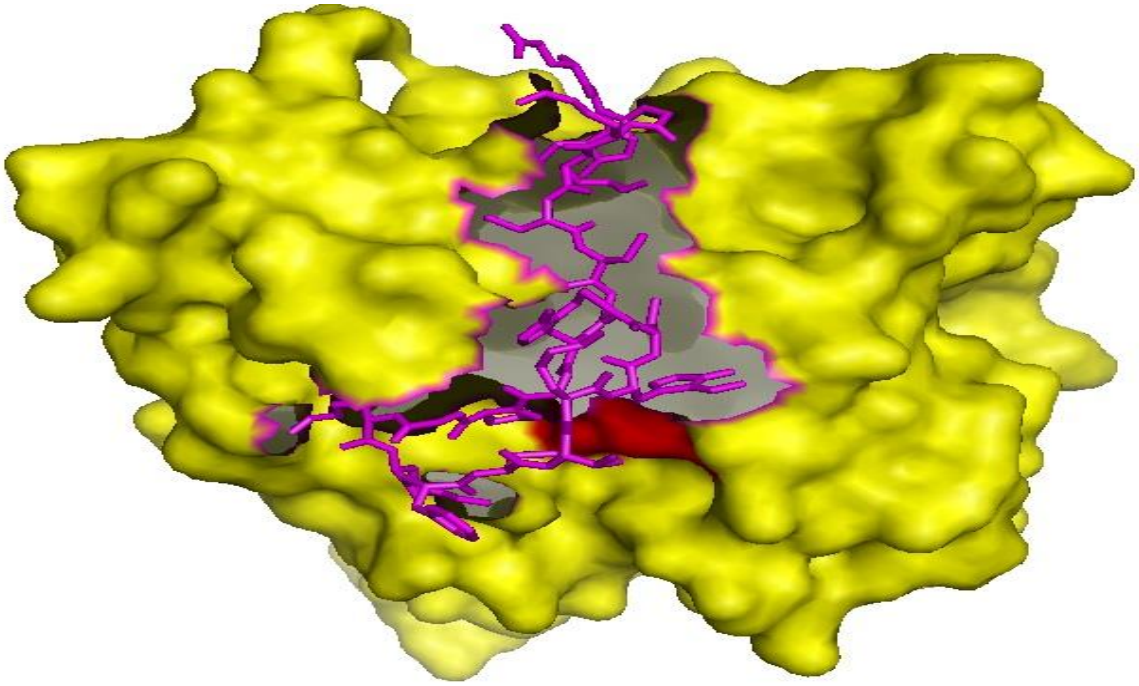

FIGURE 4.15: The figure shows best docked structure of ETB and Ib-AMP1. The residues of ETA are shown in yellow colour and the residues of Ib-AMP1 are shown in magenta. The red coloured residues show the crucial residues of ETB.

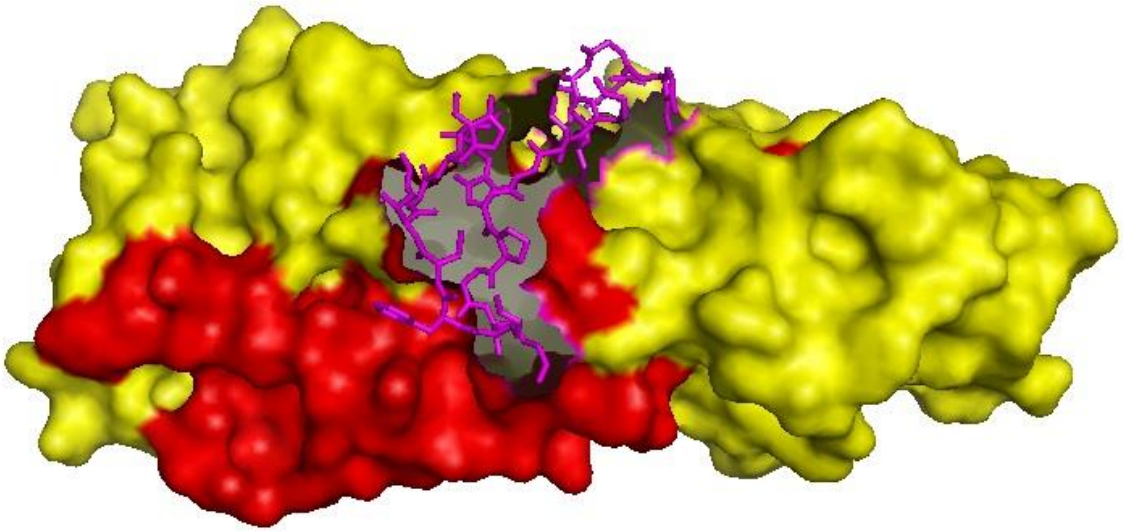

FIGURE 4.16: The figure shows best docked structure of PVL and Ib-AMP1. The residues of ETA are shown in yellow colour and the residues of Ib-AMP1 are shown in magenta. The red coloured residues show the crucial residues of PVL.

The best docked complex of docking PVL with Ib-AMP1 (shown in FIGURE 4.16) gave a global energy -22.15 kcal/mol. Total eight non-bond interactions were formed between the residues of PVL and Ib-AMP1 in this complex. Asp168 residue of PVL forms Salt-bridge with Gln1 residue of Ib-AMP1. Lys155, Arg271 and Gln104 residues of PVL form hydrogen bond with Arg5, Gln1 and Arg13 residues respectively of Ib-AMP1. Gln246 and Tyr99 residue of PVL form carbon hydrogen bond with Arg4 and Arg18 residues respectively of Ib-AMP1. Lys81 residue of PVL forms alkyl interaction with Cys6 residue of Ib-AMP1. Leu153 residue of PVL forms Pi-Alkyl interaction with Trp9 residue of Ib-AMP1.

TABLE 4.2: Crucial residues of toxins interacting with the antimicrobial peptides in the best docked complexes of *S. aureus* toxins from all the sets of dockings

Antimicrobial peptides	**Toxins**	**Crucial residues of Toxins interacting with antimicrobial peptides**
JCpep7	ETA	None
	ETB	None
	PVL	None
Sesquin	ETA	None
	ETB	None
	PVL	None
Snakin-2	ETA	None
	ETB	None
	PVL	None
Ib-AMP1	ETA	His72 Asp120

	ETB	Ser202
	PVL	Tyr99 Gln104 Leu153

4.1.3 DISCUSSION

All the docking sets were analysed for bet docking complexes. Analysis of the docking of ETA with all the four antimicrobial peptides it was seen that the best global energy was given by the docking complex between ETA and Snakin-2. Four hydrogen bonds were formed in this complex and the complex had a global energy of -47.39 kcal/mol. Comparisons of the best docking complexes from each set of docking, found after docking ETB with the four antimicrobial peptides, showed that the best global energy was found in docked complex between ETB and JCpep7. The complex had a global energy of -18.28 kcal/mol and two hydrogen bonds were formed between ETB and JCpep7. The best global energy of found after comparing the docking sets of the antimicrobial peptides with PVL was that of a docked complex between PVL and Snakin-2. Although the global energy in this case was minimum, i.e., -24.96kcal/mol, but no hydrogen bonds were formed between Snakin-2 and PVL.

After analysis of the interacting residues of the docked complexes with the antimicrobial peptides, it was seen that Ib-AMP1 interacted with maximum number of crucial residues as compared to the other antimicrobial peptides (as shown in TABLE 4.2). Ib-AMP1 also showed significant global energies and interactions with all the three toxins of *S. aureus* (as shown in TABLE 4.1). Ib-AMP1 is the only antimicrobial peptide that interacts with the crucial residues of the toxins ETA, ETB and PVL.

4.2 Studies of interaction of antimicrobial peptides with *Vibrio cholerae* transcription activator ToxT

4.2.1 ToxT modelled

The 3D structure of ToxT in 3GBG had missing residues from 100-109. Thus the structure of ToxT had to be modelled using I-TASSER. I-TASSER returned two models, i.e. model-1 and model-2, as output. Model-1 has C-score 0.93, estimated TM-score was 0.84±0.08 and estimated RMSD was 4.1±2.8 Å. Model-2 has a C-score -1.49. Model-1 was selected for further studies based upon C-score, TM-score and RMSD. Now the modelled structure was a 3D structure with all the amino acids complete in the chain. The predicted secondary structure from I-TASSER predicts the model to consist of nine beta-strands and ten alpha helices. The missing residues of ToxT form an alpha helix in continuation with the existing alpha-helix in the modelled structure.

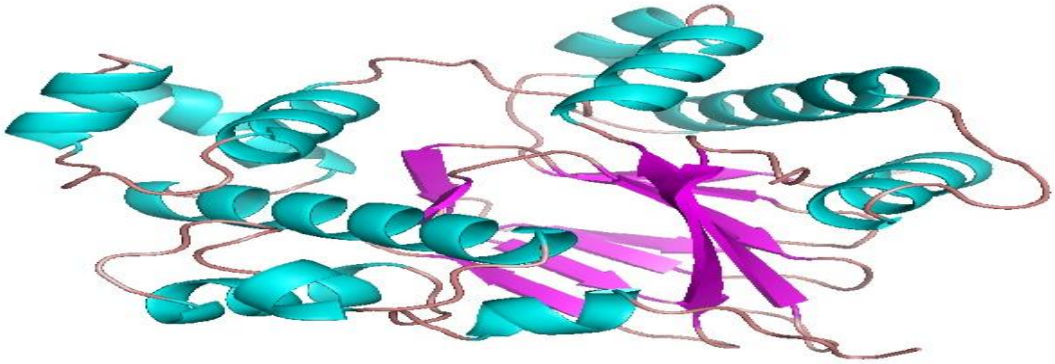

FIGURE 4.17: The figure shows the modelled structure of ToxT with the missing residues repaired in it. Alpha helices are shown in cyan and beta strands are shown in magenta.

4.2.2 Docking results

4.2.2.1 Docking of ToxT with Ib-AMP1

The best docking complex of interaction of ToxT with Ib-AMP1 (shown in FIGURE 4.18)

shows protein-peptide interaction energy -54.55 kcal/mol. Two salt bridges are formed between Arg187 and Asp113 residues of ToxT and Cys20 and Gln1 residues respectively of Ib-AMP1. Arg221 and Asp44 residues of ToxT form electrostatic interactions with Cys20 and Arg4 residues respectively of Ib-AMP1. Arg187 and Cys63 residues of ToxT form hydrogen bond with Arg18 and Gln1 residues respectively of Ib-AMP1. Tyr250 and Thr253 of ToxT form hydrogen bond with Arg14 residue of Ib-AMP1. Arg68 residue of ToxT forms two pi-cation interactions with Trp9 residue of Ib-AMP1. Glu215 residue of ToxT forms Pi-anion interaction with Trp9 residue of Ib-AMP1. Tyr250 residue of ToxT forms Pi-Donor hydrogen bond interaction with Cys20 residue of Ib-AMP1. Arg68 residue of ToxT forms Pi-Sigma interaction with Trp9 residue of Ib-AMP1. Tyr250, Ile66 and Arg68 residues of ToxT form Pi- Alkyl interaction with Cys16, Trp2 and Trp9 residues respectively of Ib-AMP1. Arg209 residue of ToxT forms two pi-alkyl interactions with Trp22 of Ib-AMP1. Arg221 and Thr253 are the crucial residues of ToxT which interact with Ib-AMP1 in this docked complex.

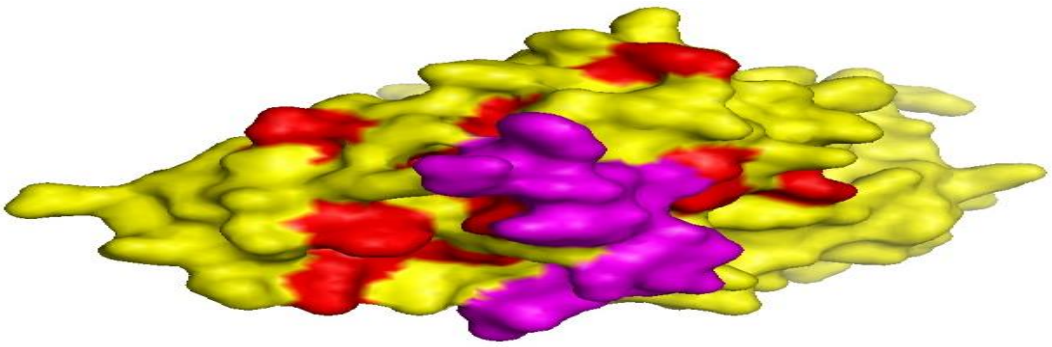

FIGURE 4.18: The figure shows the docked complex of ToxT and Ib-AMP1. The yellow residues represent the residues of ToxT, red residues represent the crucial residues of ToxT and the magenta residues represent the residues of antimicrobial peptide Ib-AMP1.

4.2.2.2 Docking of ToxT with Ib-AMP2

The best docking complex of interaction of ToxT with Ib-AMP2 (shown in FIGURE 4.19)

shows protein-peptide interaction energy -49.46 kcal/mol. In this complex Glu172 residue of ToxT forms a salt bridge with Arg18 residue of Ib-AMP2. Asp167 residue of ToxT forms electrostatic interaction with Arg18 residue of Ib-AMP2. Asn28 and Ser175 residues of ToxT form hydrogen bonds with Cys20 residue of Ib-AMP2. Asn173, Lys5, Tyr224, Asp88 and Asp29 residues of ToxT forms hydrogen bond with Cys16, Cys7, Gln1, Asn8 and Trp19 residues respectively of Ib-AMP2. Asp88 residue of ToxT forms Pi-Anion interaction with Trp19 residue of Ib-AMP2. Cys176 and Lys173 residues of ToxT form alkyl interactions with Cys16 residue of Ib-AMP2. Cys176 and Lys179 residues of ToxT form alkyl interaction with Cys20 residue of Ib-AMP2. Cys176, Leu228 and Lys5 residues of ToxT form alkyl interactions with Arg18, Arg4 and Cys7 residues respectively of Ib-AMP2. Lys5 residue of ToxT forms two Pi-Alkyl interactions with Trp9 residue of Ib-AMP2. Tyr244 residue of ToxT forms Pi-Alkyl interaction with Arg4 residue of Ib-AMP2. Ser175 is the crucial residue of ToxT interacting with Ib-AMP2 in this docked complex.

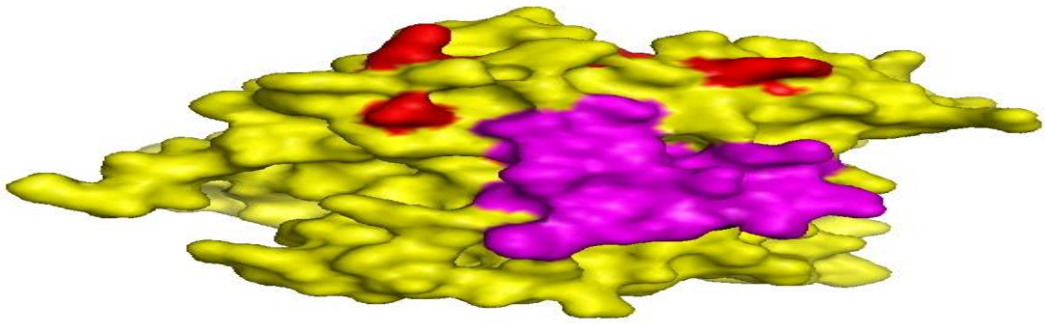

FIGURE 4.19: The figure shows the docked complex of ToxT and Ib-AMP2. The yellow residues represent the residues of ToxT, red residues represent the crucial residues of ToxT and the magenta residues represent the residues of antimicrobial peptide Ib-AMP2.

4.2.2.3 Docking of ToxT with Ib-AMP3

The best docking complex of interaction of ToxT with Ib-AMP3 (shown in FIGURE 4.20) shows protein-peptide interaction energy -41.39 kcal/mol. Glu215 residue of ToxT forms salt

bridge with Arg13 residue of Ib-AMP3. Trp186 and Gly244 residues of ToxT form hydrogen bonds with Gln1 residue of Ib-AMP3. Arg68, Arg214 and Ser257 residues of ToxT form hydrogen bonds with Gly12, Ala8 and Tyr291 residues respectively of Ib-AMP3. Ser257 and Asn23 residues of ToxT form carbon hydrogen bond with Lys14 residue of Ib-AMP3. Glu215 residue of ToxT form carbon hydrogen bond with Arg13 residue of Ib-AMP3. Tyr250 residue of ToxT form Pi donor hydrogen interaction with Trp9 residue of Ib-AMP3. Tyr250 residue of ToxT form Pi sulphur interaction with Cys16 residue of Ib-AMP3. Tyr 250 residue of ToxT forms Pi-Pi stacked interaction with Tyr2 residue of Ib-AMP3. Val254 residue of ToxT forms Alkyl interaction with Lys14 residue of Ib-AMP3. Tyr250 and Arg214 residues of ToxT form Pi Alkyl interaction with Cys6 and Trp9 residues respectively of Ib-AMP3. Trp186, Arg214, Gly244 and Ser257 are the crucial residues of ToxT interacting with Ib-AMP3 in this docked complex.

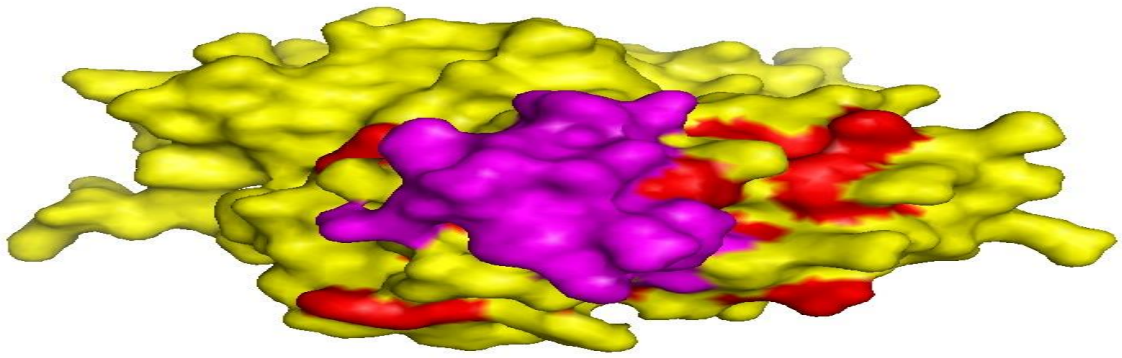

FIGURE 4.20: The figure shows the docked complex of ToxT and Ib-AMP3. The yellow residues represent the residues of ToxT, red residues represent the crucial residues of ToxT and the magenta residues represent the residues of antimicrobial peptide Ib-AMP3.

4.2.2.4 Docking of ToxT with Ib-AMP4

The best docking complex of interaction of ToxT with Ib-AMP4 (shown in FIGURE 4.21) shows protein-peptide interaction energy -44.13 kcal/mol. Asp44 residue of ToxT forms two

electrostatic interactions with Arg13 residue of Ib-AMP4. Asp113 residue of ToxT forms electrostatic interaction with Arg13 and Arg14 residues of Ib-AMP4. Glu110 residue of ToxT forms electrostatic interaction with Arg17 residue of Ib-AMP4. Cys47, Ala170, Lys204, Ser208, Arg68 and Glu110 residues of ToxT forms hydrogen bond with Gly12, Tyr15, Cys7, Cys16, Arg13 and Arg17 residues respectively of Ib-AMP4. Ser208 residue of ToxT forms hydrogen bond with Arg14 residue of Ib-AMP4. Asp169 residue of ToxT forms Pi-Anion interaction with Tyr15 residue of Ib-AMP4. Asp166 residue of ToxT forms Pi- Sigma interaction with Trp2 residue of Ib-AMP4. Met171 residue of ToxT forms Pi-Sulfur interaction with Tyr15 residue of Ib-AMP4. Cys47 and Lys204 residues of ToxT form alkyl interaction with Arg13 and Cys16 residues respectively of Ib-AMP4. Ala170 residue of ToxT form Pi-Alkyl interaction with Tyr15 residue of Ib-AMP4. Leu102 and Lys95 residues of ToxT form Pi-Alkyl interaction with Trp2 residue of Ib-AMP4. None of the crucial residues of ToxT interact with Ib-AMP4 in this docked complex.

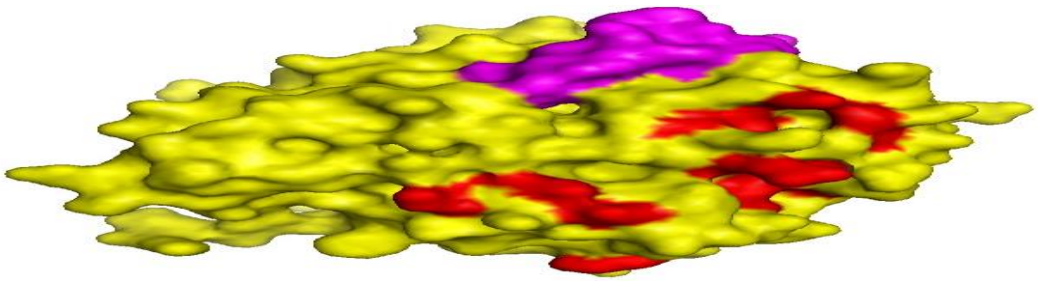

FIGURE 4.21: The figure shows the docked complex of ToxT and Ib-AMP4. The yellow residues represent the residues of ToxT, red residues represent the crucial residues of ToxT and the magenta residues represent the residues of antimicrobial peptide Ib-AMP4.

After studying the non-bond interactions of the best docked complexes of all the sets of docking, it was predicted that the best docking interactions were shown by the docked complexes formed with antimicrobial peptides Ib-AMP1 and Ib-AMP3. These docked complexes were further taken for molecular dynamics studies.

4.2.3 Molecular dynamics simulation results

Molecular dynamics simulation was carried out using GROMACS. The modelled 3D structure of ToxT, docked complex of ToxT-Ib-AMP1 and docked complex of ToxT-Ib-AMP3 were simulated for 10ns. The values of root mean square deviation (RMSD), root mean square fluctuation (RMSF) and radius of gyration (Rg) for the above simulations were compared.

The total charge on ToxT, docked complex of ToxT+Ib-AMP1 and docked complex of ToxT+Ib-AMP3 was 5, 10 and 11 respectively. These charges were neutralized by adding 5, 10 and 11 chloride ions to ToxT, docked complex of ToxT+Ib-AMP1 and docked complex of ToxT+Ib-AMP3 respectively. On comparing the RMSD values of the above three simulations (shown in FIGURE 4.22), it was seen that the values of RMSD of ToxT+Ib-AMP3 show a great fluctuations in the values from 0ns to 10ns. This shows that the docked complex formed between ToxT and Ib-AMP3 is unstable. When comparing the RMSD values of ToxT and docked complex of ToxT+Ib-AMP1 (shown in FIGURE 4.23), it was seen that the RMSD values of ToxT were less than the RMSD values of the docked complex of ToxT+Ib-AMP1. It is observed that the values of RMSD for docked complex of ToxT+ Ib-AMP1 shows an increase from 0ns to 3.3ns. After that the values of RMSD become nearly stable with very less fluctuations. Whereas, the RMSD values of ToxT show an increase from 0ns to 2ns. The values of RMSD further show stability with less fluctuation till 6.7ns nearly. After that the values of RMSD do not show any stability, these keep on increasing. Thus, with the above observations on the basis of RMSD analysis it can be predicted that the docked complex formed between ToxT and Ib-AMP1 is much more stable than the ToxT alone.

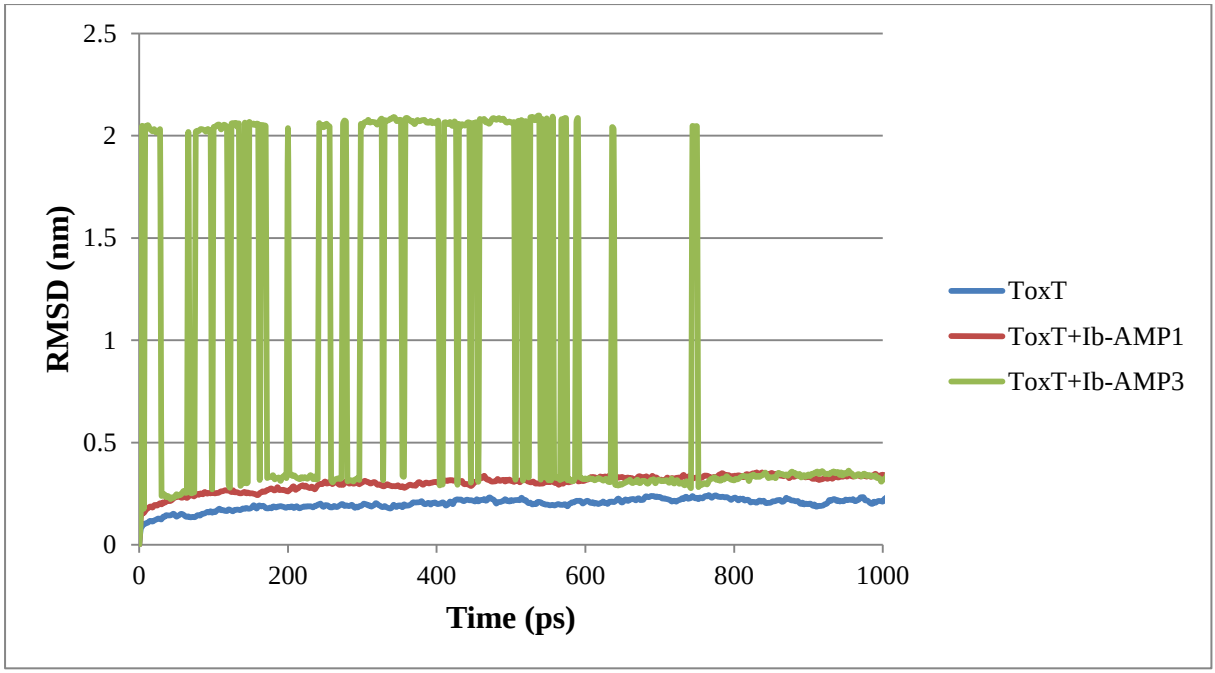

FIGURE 4.22: Comparative plot for the RMSD values of ToxT, docked complex of ToxT+Ib-AMP1 and docked complex of ToxT+Ib-AMP3.

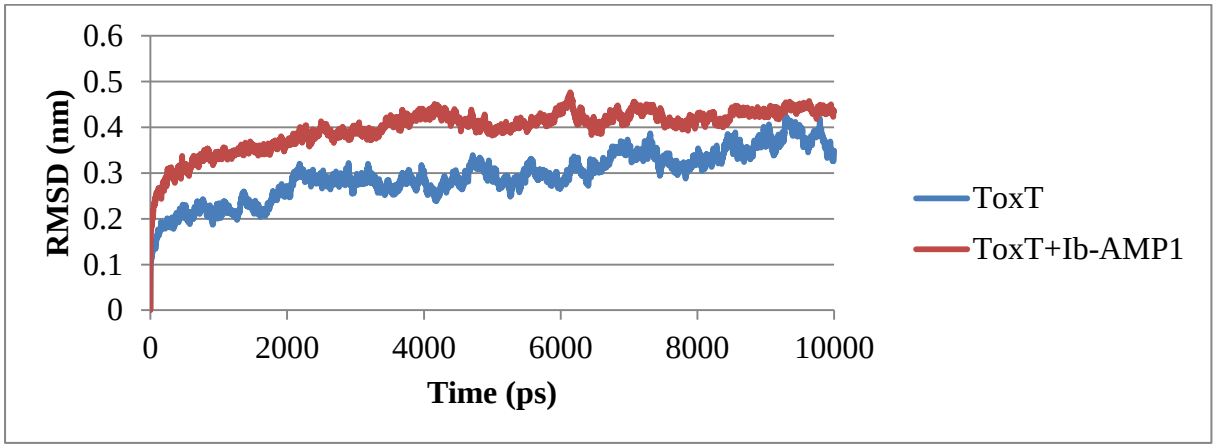

FIGURE 4.23: Comparative plot for the RMSD values of ToxT and docked complex of ToxT+Ib-AMP1. The red line of RMSD plot of docked complex of ToxT and Ib-AMP1 shows the most stability.

The comparison of RMSF values of ToxT, docked complex of ToxT+Ib-AMP1 and docked complex of ToxT+Ib-AMP3 (shown in FIGURE 4.24) shows high fluctuations of RMSF values for docked complex of ToxT+Ib-AMP3. Since, the fluctuations of the atoms show

high values thus the stability of atoms decreases and hence, the docked complex of ToxT+Ib-AMP3 is unstable. The values of RMSF for ToxT and ToxT+Ib-AMP1 show that the fluctuations of most of the atoms is less in the docked complex as compared to the protein ToxT simulated alone. It was seen that fluctuations of the crucial residues of ToxT and those residues of ToxT involved interactions with Ib-AMP1 show a decrease in the docked complex. Thus, it can be predicted that the fluctuations of atoms about their mean positions decreases when ToxT is docked with Ib-AMP1. Hence, the docked complex formed is much more stable than the protein ToxT.

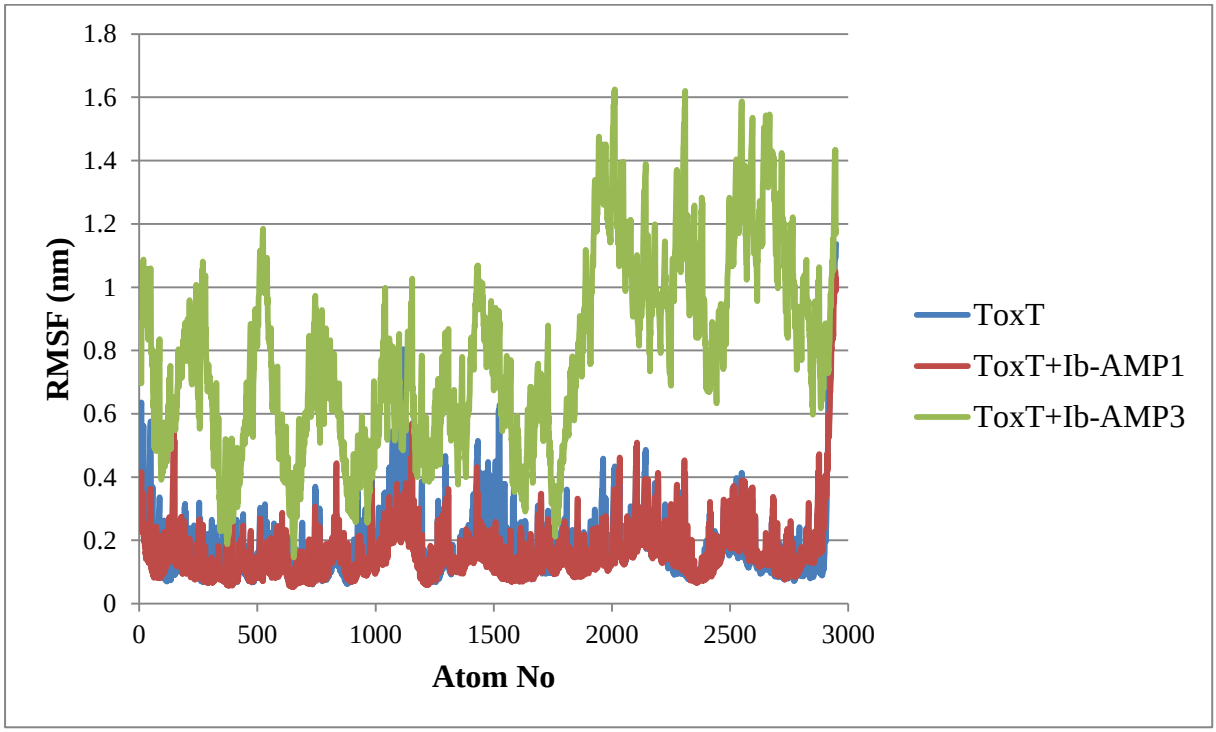

FIGURE 4.24: Comparative plot for the RMSF values of ToxT, docked complex of ToxT+Ib-AMP1 and docked complex of ToxT+Ib-AMP3. The predicted structural stability of the complex of ToxT and Ib-AMP1 is maximum among these.

The comparison of values of radius of gyration for ToxT, docked complex of ToxT+Ib-AMP1 and docked complex of ToxT+Ib-AMP3 (shown in FIGURE 4.25), show great fluctuations in the values for the docked complex ToxT+Ib-AMP1. The values of radius of

gyration for ToxT alone show more fluctuations as compared to the values of the docked complex of ToxT and Ib-AMP1 (shown in FIGURE 4.26). This reveals that the docked complex of ToxT and Ib-AMP1 is much more compact as compared to the structure of ToxT. The comparison of the above three sets of values for radius of gyration reveal that the docked structure of ToxT and Ib-AMP1 shows most compactness and thus is most stable structure. Thus it is predicted that the compactness and thus the stability of ToxT increases when docked with Ib-AMP1.

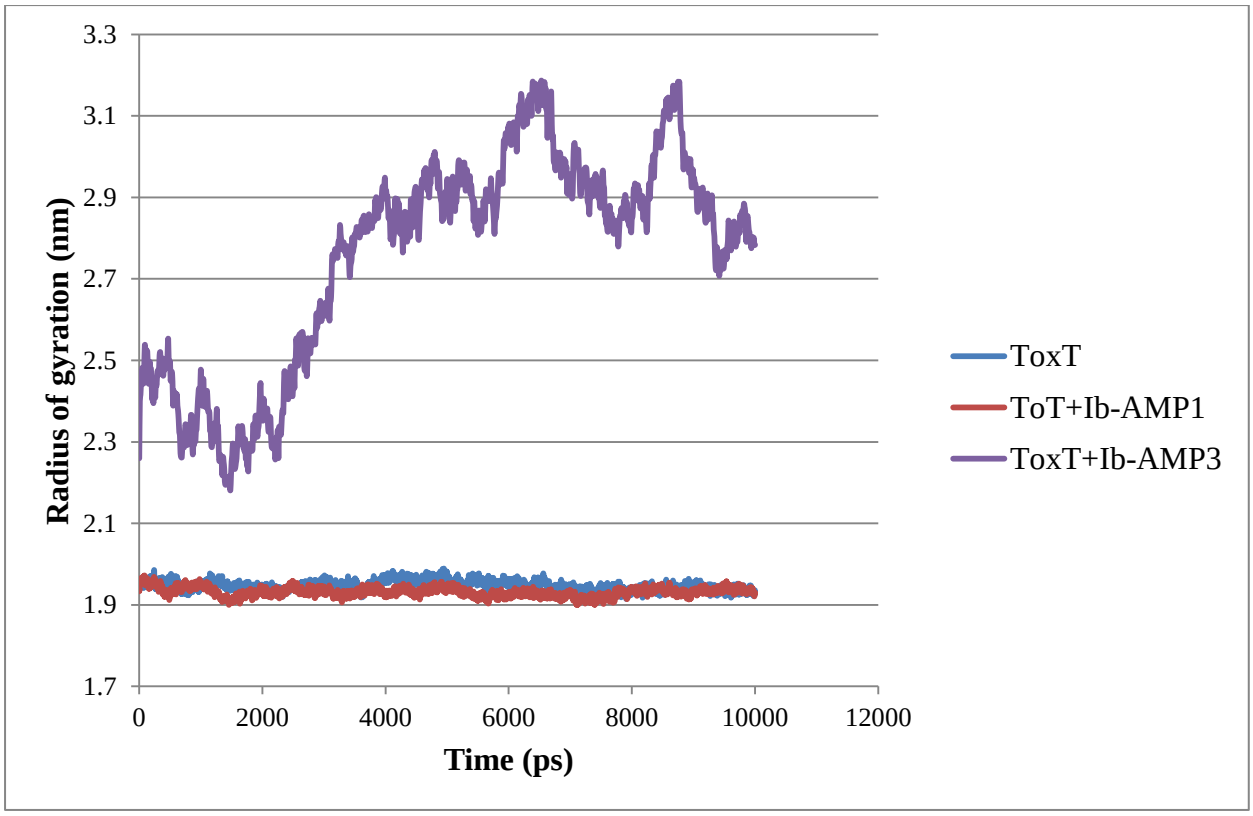

FIGURE 4.25: Comparative plot for the Radius of gyration values of ToxT, docked complex of ToxT+Ib-AMP1 and docked complex of ToxT+Ib-AMP3. Time is shown in ps and radius of gyration in nm.

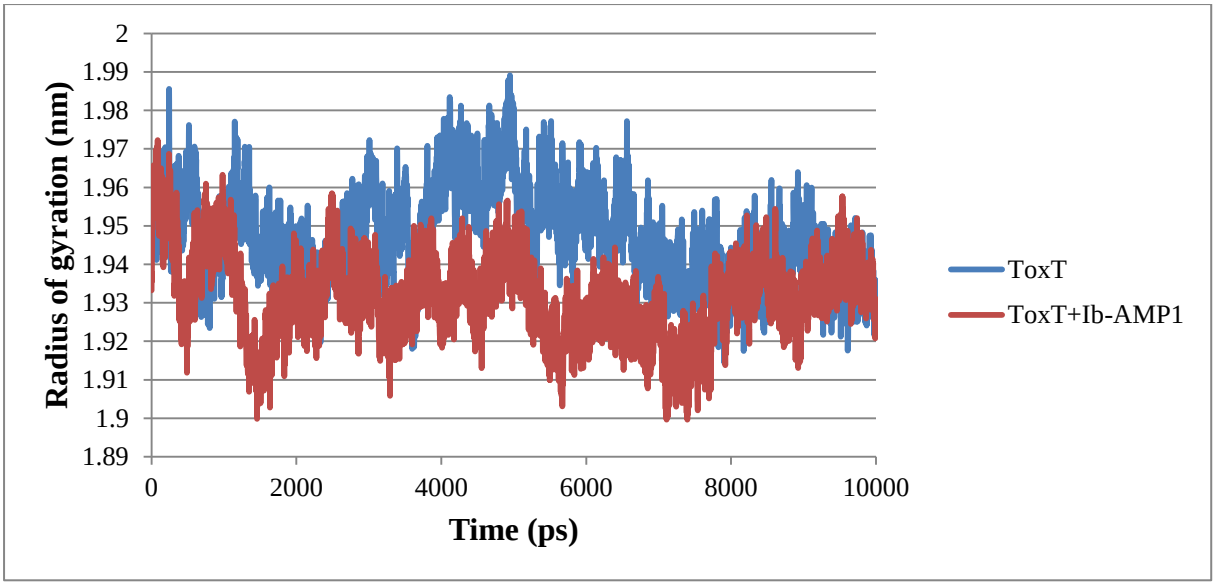

FIGURE 4.26: Comparative plot for the Radius of gyration values of ToxT and docked complex of ToxT+Ib-AMP1. The predicted compactness of structure of docked complex of ToxT and Ib-AMP1 is more than that of ToxT.

4.2.4 ProtParam prediction of Ib-AMP1

TABLE 4.3: In silico characterization of antimicrobial peptide Ib-AMP1

Sequence	QWGRRCCGWG PGRRYCVRWC
Molecular weight	2485.91 Da
Theoretical pI	9.88
Charge	+5
Formula	$C_{107}H_{157}N_{39}O_{23}S_4$
Total no. of atoms	330

4.2.5 ToxinPred prediction of Ib-AMP1

The sequence of Ib-AMP1 was given as input to the ToxinPred server and the output

predicted Ib-AMP1 as Toxic. Thus, this was predicted unsuitable for development as alternate drug. Likewise all the other three antimicrobial peptides were given as input to ToxinPred. All these three peptides were also predicted as Toxic. Thus none of the above four antimicrobial peptides from *Impatiens balamina* were suitable for development as alternate drug.

4.2.6 DISCUSSION

The predicted model of ToxT predicted the secondary structure at nearly the same regions where they were present in 3GBG. The predicted structure was used for further studies. Of all the four antimicrobial peptides Ib-AMP1, Ib-AMP2, Ib-AMP3 and Ib-AMP4 of *Impatiens balsamina*, the antimicrobial peptide Ib-AMP1 gives the least protein-peptide binding energy on docking with ToxT, i.e., -54.55 kcal/mol with two crucial residues of ToxT, i.e., Arg221 and Thr253 interacting with Ib-AMP1. Ib-AMP2 interacts with one crucial residue of ToxT ,i.e. Ser175, and the docked structure has a protein-peptide interaction energy of -49.46 kcal/mol. Ib-AMP3 interacts with Trp186, Arg214, Gly244 and Ser257 residues of ToxT and the docked complex has a protein-peptide interaction energy of -41.39 kcal/mol. Ib-AMP4 interacts with no crucial residue of ToxT and the docked structure has a protein-peptide interaction energy of -44.13 kcal/mol. On the basis of interaction of antimicrobial peptides with the crucial residues of ToxT, the docked complexes of ToxT+Ib-AMP1 and ToxT+Ib-AMP3 were considered for further simulation studies. The comparison of RMSD values of ToxT, docked complex of ToxT+Ib-AMP1 and docked complex of ToxT+Ib-AMP3 showed minimum fluctuations for the docked complex of ToxT+Ib-AMP1. The comparison of RMSF values of ToxT, docked complex of ToxT+Ib-AMP1 and docked complex of ToxT+Ib-AMP3 showed minimum fluctuations for atoms of crucial residues of ToxT for docked complex of ToxT+Ib-AMP1. Thus, it is seen that the stability of protein ToxT increases when it binds to the antimicrobial peptide Ib-AMP1. The comparison of Radius of gyration values

of ToxT, docked complex of ToxT+Ib-AMP1 and docked complex of ToxT+Ib-AMP3 showed that the values of radius of gyration shows least fluctuations for the docked complex of ToxT+Ib-AMP1. Thus, it is seen that protein ToxT becomes more compact when it binds with antimicrobial peptide Ib-AMP1.

4.3 Selection of potential antimicrobial peptide against Diphtheria toxin

4.3.1 3D structures of antimicrobial peptides

The 3D structures of antimicrobial peptides predicted from Pepfold3 are shown below. The antimicrobial peptides are short length; hence their 3D structures are also very flexible.

4.3.1.1 Anionic peptide SAAP

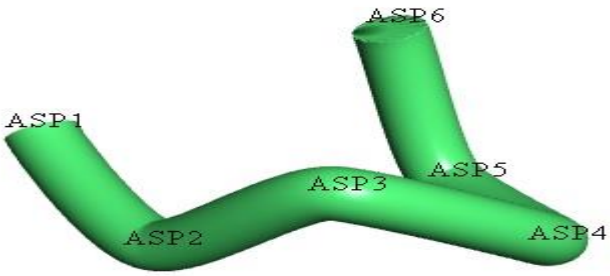

FIGURE 4.27: Predicted 3D structure of Anionic peptide SAAP

4.3.1.2 Bacteriocin

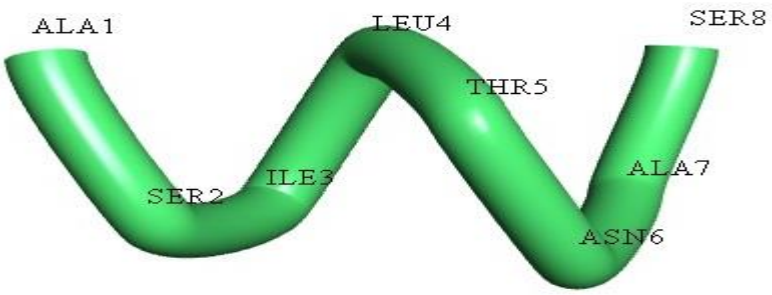

FIGURE 4.28: Predicted 3D structure of Bacteriocin

4.3.1.3 Curvalicin-28c

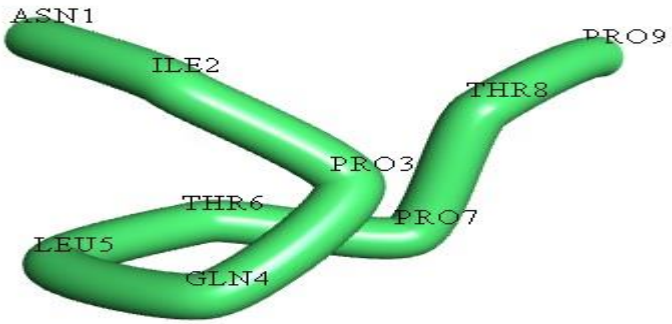

FIGURE 4.29: Predicted 3D structure of Curvalicin-28c

4.3.1.4 NRWC

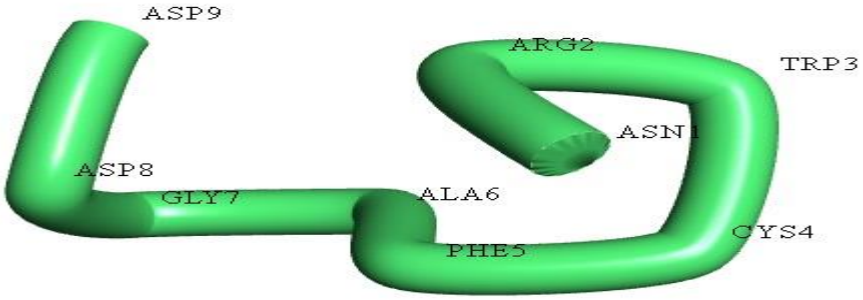

FIGURE 4.30: Predicted 3D structure of NRWC

4.3.1.5 JCpep7

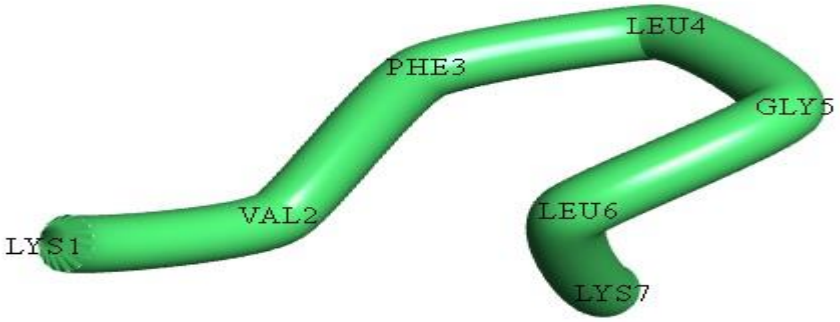

FIGURE 4.31: Predicted 3D structure of JCPep7

4.3.1.6 Antimicrobial peptide1

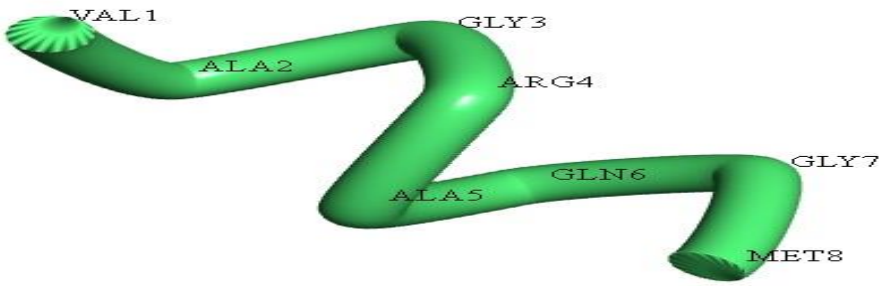

FIGURE 4.32: Predicted 3D structure of Antimicrobial peptide 1

4.3.1.7 Cr-ACP1

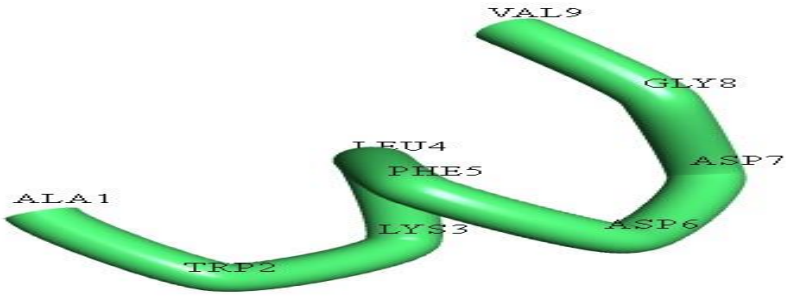

FIGURE 4.33: Predicted 3D structure of Cr-ACP1

4.3.1.8 Sesquin

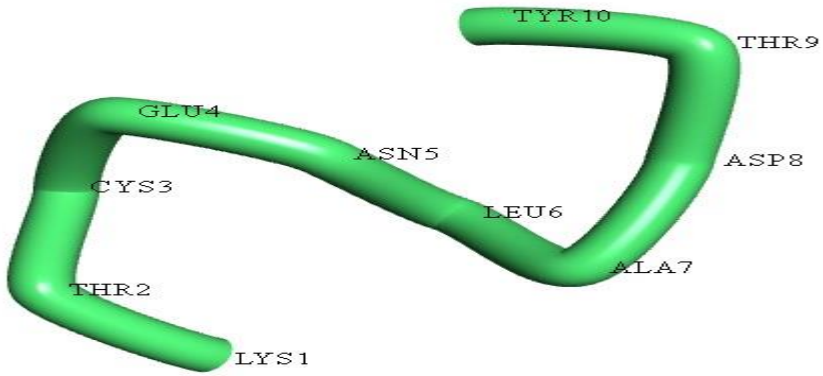

FIGURE 4.34: Predicted 3D structure of Sesquin

4.3.1.9 Alliumin

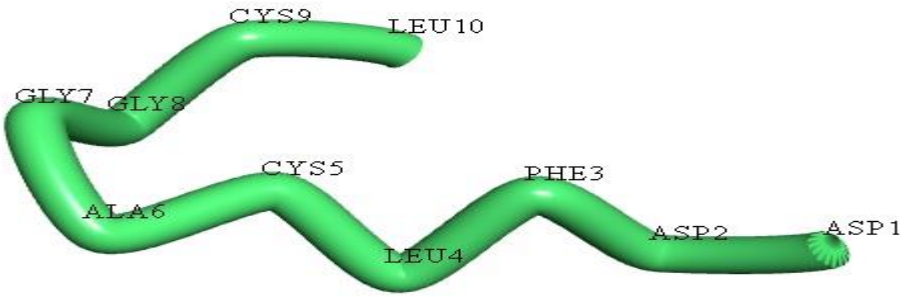

FIGURE 4.35: Predicted 3D structure of Alliumin

4.3.2 Docking results

4.3.2.1 Docking interactions of catalytic domain of diphtheria toxin with the antimicrobial peptides from microorganisms

4.3.2.1.1 Docking interactions of DT with SAAP

The best docked complex (shown in FIGURE 4.36), formed after docking interaction between catalytic domain of diphtheria toxin and SAAP, has a global energy -19.11 kcal/mol. Lys24 residue of the catalytic domain of diphtheria toxin form salt bridge with Asp5 residue of SAAP. Lys24 residue of catalytic domain of diphtheria toxin form electrostatic bond with

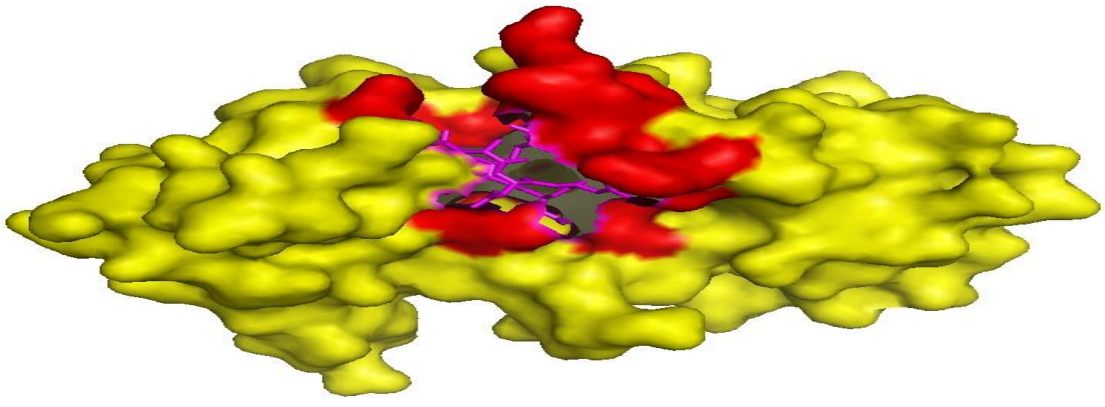

FIGURE 4.36: The figure shows the docked complex of DT and SAAP. The yellow residues represent the residues of DT, red residues represent the crucial residues of DT and the magenta residues represent the residues of antimicrobial peptide SAAP.

Asp2 residue of SAAP. Gln43, Tyr65 and Asn69 residues of catalytic domain of diphtheria toxin form hydrogen bond with Asp6, Asp4 and Asp1 residues respectively of SAAP. His21 and Phe53 residues of catalytic domain of diphtheria toxin form carbon hydrogen bond with Asp4 and Asp6 residues respectively of SAAP. His21 and Tyr46 residues of catalytic domain of diphtheria toxin form Pi- Anion interaction with Asp5 and Asp3 residues respectively of SAAP.

4.3.2.1.2 Docking interactions of DT with Microcin C7

The best docked complex (shown in FIGURE 4.37), formed after docking interaction between catalytic domain of diphtheria toxin and Microcin C7, has a global energy −43.23 kcal/mol. Gly22, Thr42 and Asn69 residues of catalytic domain of diphtheria toxin form conventional hydrogen bonds with Ala6, MSE1 and MSE1 residues respectively, of Microcin C7. His21 and Ala62 of catalytic domain of diphtheria toxin form carbon hydrogen bond with Asn5 and Asn7 residues respectively, of Microcin C7. Tyr65 of diphtheria toxin forms electrostatic interaction with Asn7 residue of Microcin C7. The Pi-orbitals of His21 of diphtheria toxin form non-bond with lone pair Ala6 residue of Microcin C7. Tyr46 and Tyr65

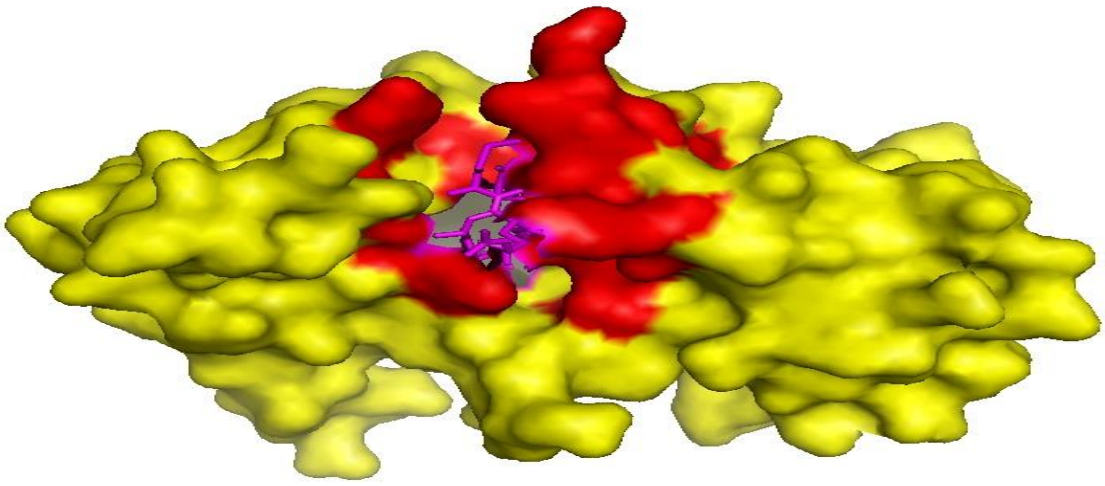

FIGURE 4.37: The figure shows the docked complex of DT and Microcin C7. The yellow residues represent the residues of DT, red residues represent the crucial residues of DT and the magenta residues represent the residues of antimicrobial peptide MicrocinC7.

of catalytic domain of diphtheria toxin form hydrophobic interaction with Arg2 and Ala6 residues respectively of Microcin C7.

4.3.2.1.3 Docking interactions of DT with Bacteriocin

The best docked complex (shown in FIGURE 4.38), formed after docking interaction between catalytic domain of diphtheria toxin and Bacteriocin, has a global energy -16.35 kcal/mol. Ser30 and Ser40 residues of catalytic domain of diphtheria toxin form conventional hydrogen bond with Ser8 and Asn6 residues respectively of Bacteriocin. Ser30 residue of catalytic domain of diphtheria toxin forms carbon hydrogen bond with Ser8 residue of Bacteriocin. Tyr27 residue of catalytic domain of diphtheria toxin form Pi-Lone pair interaction with Leu4 residue of Bacteriocin. Tyr27 residue of catalytic domain of diphtheria toxin forms amide-pi stacked interaction with Asn6 and Ala7 residues of Bacteriocin. Ile31 and Lys24 residues of catalytic domain of diphtheria toxin form alkyl interaction with Leu4 and Ala1 residues respectively of Bacteriocin. Pro38 residue of catalytic domain of diphtheria toxin forms Alkyl interactions with Ile3 and Ala7 residues of Bacteriocin. His21 and Trp153 residues of catalytic domain of diphtheria toxin form Pi-alkyl interactions with Leu4 and Ile3 residues respectively of Bacteriocin.

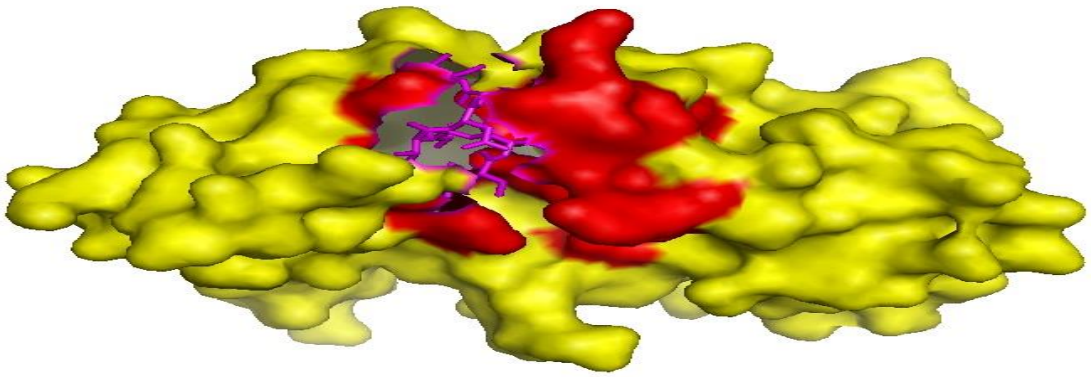

FIGURE 4.38: The figure shows the docked complex of DT and Bacteriocin. The yellow residues represent the residues of DT, red residues represent the crucial residues of DT and the magenta residues represent the residues of antimicrobial peptide Bacteriocin.

4.3.2.1.4 Docking interactions of DT with Curvalicin-28c

The best docked complex (shown in FIGURE 4.39), formed after docking interaction between catalytic domain of diphtheria toxin and Curvalicin-28c, has a global energy -47.39 kcal/mol. Asn69 residue of catalytic domain of diphtheria toxin forms hydrogen bond with Thr6 residue of Curvalicin-28c. Asn69 residue of catalytic domain of diphtheria toxin forms carbon hydrogen bond with Thr8 and Pro9 residues of Curvalicin-28c. Pro38 residue of catalytic domain of diphtheria toxin forms hydrogen bond with Gln4 residues of Curvalicin-28c. Pro38 residue of catalytic domain of diphtheria toxin forms alkyl interaction with Leu5 residue of Curvalicin-28c. Tyr27 and Tyr46 residues of catalytic domain of diphtheria toxin form Pi-Alkyl interaction with Leu5 and Pro7 residues respectively of Curvalicin-28c.

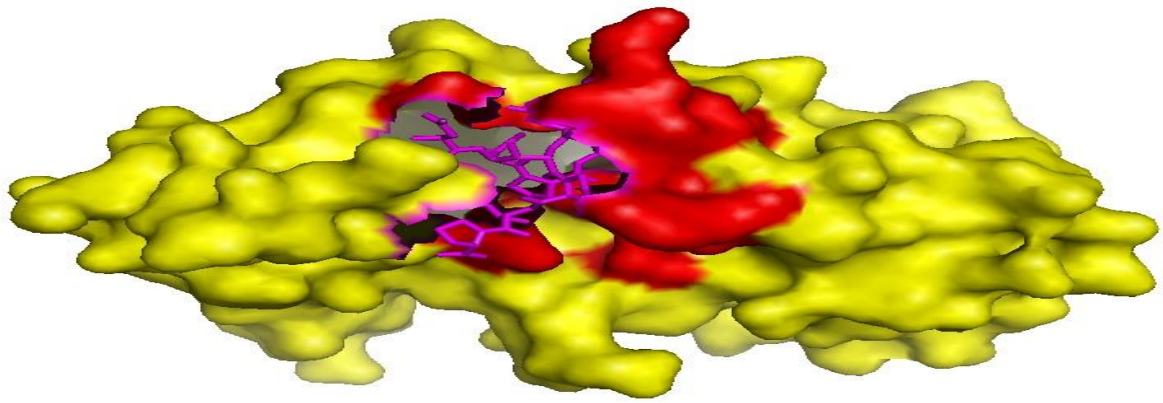

FIGURE 4.39: The figure shows the docked complex of DT and Curvalicin-28c. The yellow residues represent the residues of DT, red residues represent the crucial residues of DT and the magenta residues represent the residues of antimicrobial peptide Curvalicin-28c.

4.3.2.1.5 Docking interactions of DT with NRWC

The best docked complex (shown in FIGURE 4.40), formed after docking interaction between catalytic domain of diphtheria toxin and NRWC, has a global energy -18.12 kcal/mol. Lys24 residue of diphtheria toxin forms hydrogen bond with Asn1 residue of NRWC. Tyr65 and Glu148 residues of diphtheria toxin form carbon hydrogen bond with Asn1 and Arg2 residues respectively of NRWC. Tyr65 residue of diphtheria toxin forms Pi-

Cation interaction with Arg2 residue of NRWC. Tyr65 residue of diphtheria toxin forms Pi-Pi Stacked interaction with Trp3 residue of NRWC. His21 residue of diphtheria toxin forms two Pi-Pi stacked interactions with Trp3 residue of NRWC. Tyr54 and Tyr65 residues of diphtheria toxin forms Pi-Alkyl interaction with Arg2 residue of NRWC. Tyr46 residue of diphtheria toxin forms Pi-Alkyl interaction with Ala6 residue of NRWC.

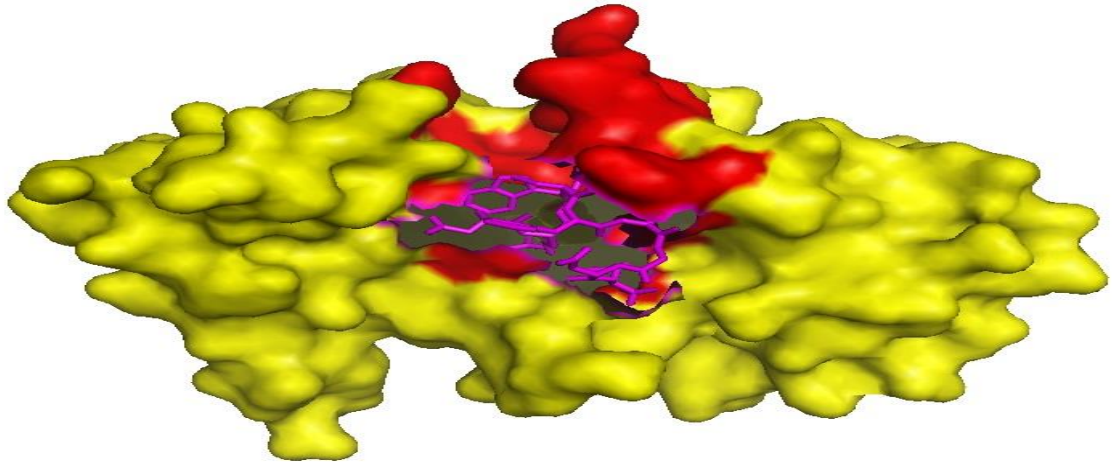

FIGURE 4.40: The figure shows the docked complex of DT and NRWC. The yellow residues represent the residues of DT, red residues represent the crucial residues of DT and the magenta residues represent the residues of antimicrobial peptide NRWC.

TABLE 4.4 : The Global energies, number of non- bond interactions and the number of hydrogen bonds formed from docking interactions of antimicrobial peptides from microorganism source and the catalytic domain of diphtheria toxin are shown.

S. No.	**AMP**	**Global Energy (kcal/mol)**	**Non Bond interactions**	**No. of H bond**
1.	SAAP	-19.11	9	3
2.	Microcin C7	**-43.23**	9	**3**
3.	Bacteriocin	-16.35	11	2
4.	Curvalicin-28c	-47.39	7	1
5.	NRWC	-18.12	10	1

The global energy of the docked complex of catalytic domain of diphtheria toxin with Curvalicin-28c is least. Considering the global energies, number of hydrogen bonds and the crucial residues of diphtheria toxin interacting with the antimicrobial peptide, the docked complex of catalytic domain of diphtheria toxin and Microcin C7 is considered best for further molecular dynamics studies.

4.3.2.2 Docking interactions of catalytic domain of diphtheria toxin with the antimicrobial peptides from plants

4.3.2.2.1 Docking interactions of DT with JC-Pep7

The best docked complex (shown in FIGURE 4.41), formed after docking interaction between catalytic domain of diphtheria toxin and JC-Pep7, has a global energy -11.60 kcal/mol. Tyr27 residue of diphtheria toxin forms hydrogen bond with Leu6 residue of JC-Pep7. Pro38 residue of diphtheria toxin forms carbon hydrogen bond with Val2 residue of JC-Pep7. Tyr27 residue of diphtheria toxin forms Pi-Sigma interaction with Val2 residue of JC-Pep7. Pro38 residue of diphtheria toxin forms Alkyl interaction with Val2 residue of JC-

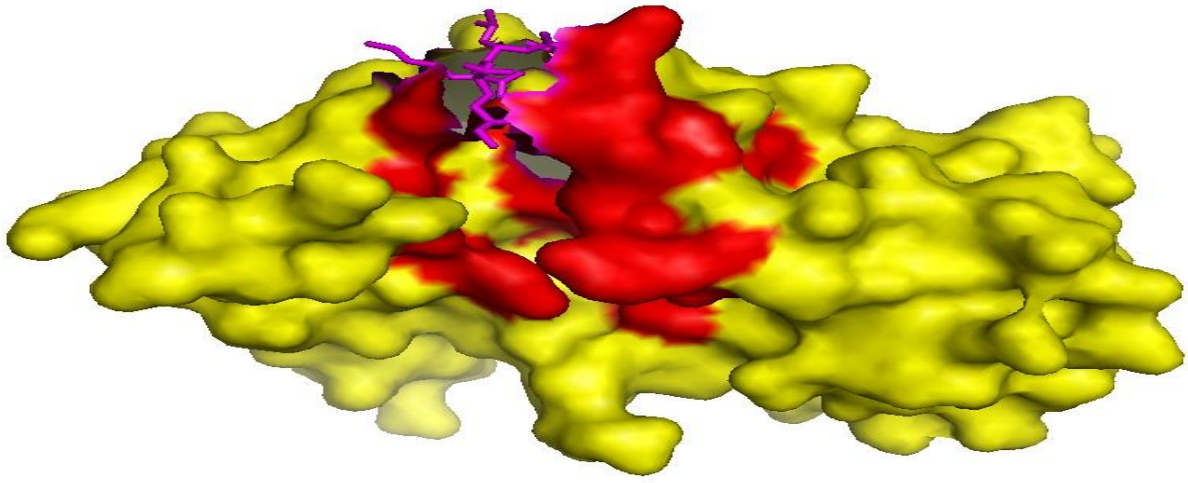

FIGURE 4.41: The figure shows the docked complex of DT and JC-Pep7. The yellow residues represent the residues of DT, red residues represent the crucial residues of DT and the magenta residues represent the residues of antimicrobial peptide JC-Pep7.

Pep7. Tyr27 and Pro38 residues of diphtheria toxin forms Pi-Alkyl interaction with Lys1 and Phe3 residues respectively of JC-Pep7.

4.3.2.2.2 Docking interactions of DT with Antimicrobial peptide1

The best docked complex (shown in FIGURE 4.42), formed after docking interaction between catalytic domain of diphtheria toxin and Antimicrobial peptide 1, has a global energy -36.92 kcal/mol. Glu70 residue of diphtheria toxin forms electrostatic interaction with Arg4 residue of Antimicrobial peptide 1. Lys24 and Gly22 residues of diphtheria toxin form hydrogen bond with Met8 residue of Antimicrobial peptide 1. Phe53 residue of diphtheria toxin forms carbon hydrogen bond with Gln6 residue of Antimicrobial peptide 1. Tyr65 residue of diphtheria toxin forms Pi Donor Hydrogen bond interaction with Met8 residue of Antimicrobial peptide 1. Tyr27 residue of diphtheria toxin forms Pi-Sigma interaction with Ala2 residue of Antimicrobial peptide 1. Tyr65 residue of diphtheria toxin forms Pi-Sulfur interaction with Met8 residue of Antimicrobial peptide 1. His21 residue of diphtheria toxin

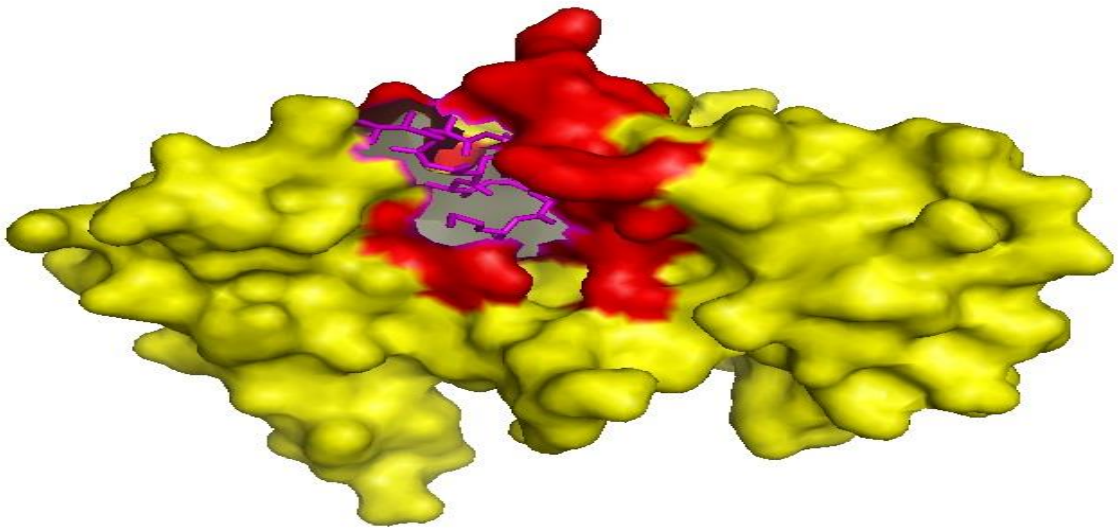

FIGURE 4.42: The figure shows the docked complex of DT and Antimicrobial peptide 1. The yellow residues represent the residues of DT, red residues represent the crucial residues of DT and the magenta residues represent the residues of antimicrobial peptide Antimicrobial peptide 1.

forms Pi-Lone pair interaction with Met8 residue of Antimicrobial peptide 1. Lys24 residue of diphtheria toxin forms alkyl interaction with Ala5 residue of Antimicrobial peptide 1. Tyr27 residue of diphtheria toxin forms Pi-Alkyl interaction with Val1 residue of Antimicrobial peptide 1.

4.3.2.2.3 Docking interactions of DT with Cr-ACP1

The best docked complex (shown in FIGURE 4.43), formed after docking interaction between catalytic domain of diphtheria toxin and Cr-ACP1, has a global energy -12.67 kcal/mol. Asp97 residue of diphtheria toxin forms electrostatic non-bond interaction with Lys3 residue of Cr-ACP1. Tyr46 residue of diphtheria toxin forms Pi-Sigma interactions with Ala1 and Leu4 residues of Cr-ACP1. Tyr46 residue of diphtheria toxin forms Pi-Alkyl interaction with Val9 residue of Cr-ACP1.

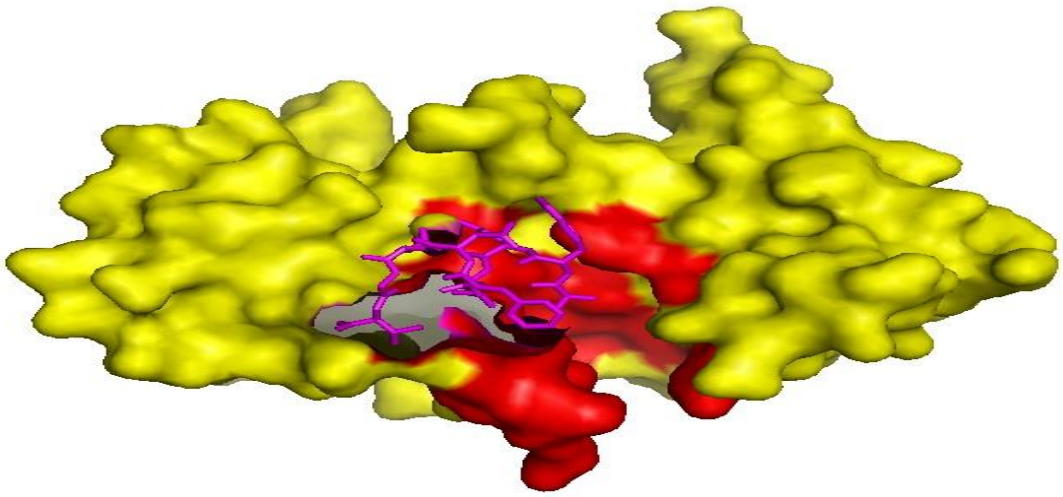

FIGURE 4.43: The figure shows the docked complex of DT and Cr-ACP1. The yellow residues represent the residues of DT, red residues represent the crucial residues of DT and the magenta residues represent the residues of antimicrobial peptide Cr-ACP1.

4.3.2.2.4 Docking interactions of DT with Sesquin

The best docked complex (shown in FIGURE 4.44), formed after docking interaction between catalytic domain of diphtheria toxin and Sesquin, has a global energy -19.31 kcal/mol. Glu70 residue of diphtheria toxin forms electrostatic non-bond interaction with

Lys1 residue of Sesquin. Asn69 and Gly52 residues of diphtheria toxin form hydrogen bond with Asn5 and Tyr10 residues respectively of Sesquin. Lys24 residue of diphtheria toxin forms carbon hydrogen bond with Thr9 residue of Sesquin. Tyr46 and Pro38 residues of diphtheria toxin form Pi-Alkyl interaction with Ala7 and Pro38 residues respectively of Sesquin.

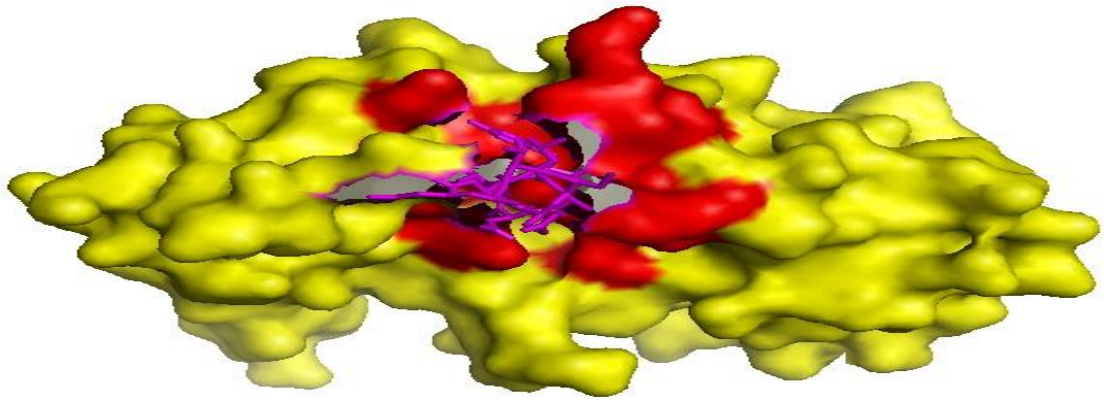

FIGURE 4.44: The figure shows the docked complex of DT and Sesquin. The yellow residues represent the residues of DT, red residues represent the crucial residues of DT and the magenta residues represent the residues of antimicrobial peptide Sesquin.

4.3.2.2.5 Docking interactions of DT with Alliumin

The best docked complex (shown in FIGURE 4.45), formed after docking interaction between catalytic domain of diphtheria toxin and Alliumin, has a global energy -31.64 kcal/mol. Lys24, Tyr54, Tyr65 and Gly44 residues of diphtheria toxin form conventional hydrogen bond with Phe3, Ala6, Gly8 and Asp2 residues respectively of Alliumin. His21 residue of diphtheria toxin form carbon hydrogen bond with Cys5 residue of Alliumin. Lys24 residue of diphtheria toxin forms Pi-Cation non-covalent interactions with Phe3 residue Alliumin. Tyr54 and Tyr65 residues of diphtheria toxin form Pi-Anion nonbond interactions with Asp1 and Leu10 residues respectively of Alliumin. Trp153 residue of diphtheria toxin form Pi-Sulphur non-bond interaction with Cys5 residue Alliumin. One Amide-Pi Stacked interaction is formed between Tyr54 residue of diphtheria toxin and Gly7, Gly8 residues of Alliumin. Lys24 residue of diphtheria toxin forms Alkyl interactions with Leu4 residue of

Alliumin. His21 residue forms Pi-Alkyl interactions with Leu10 residue of Alliumin. Two Pi-Alkyl interactions are formed between Trp153 residue of diphtheria toxin and Ala6 residue of Alliumin.

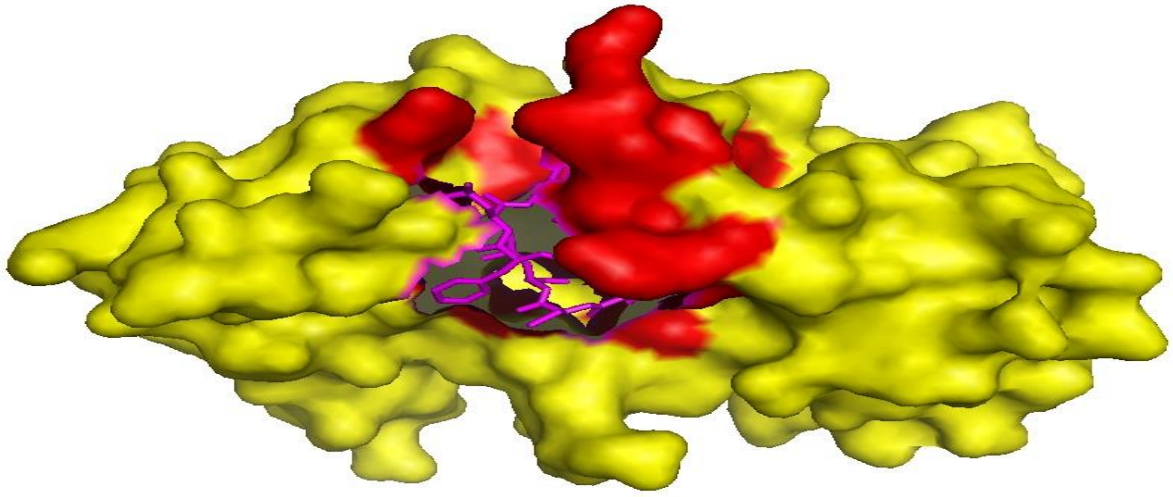

FIGURE 4.45: The figure shows the docked complex of DT and Alliumin. The yellow residues represent the residues of DT, red residues represent the crucial residues of DT and the magenta residues represent the residues of antimicrobial peptide Alliumin.

TABLE 4.5 : The Global energies, number of non- bond interactions and the number of hydrogen bonds formed from docking interactions of antimicrobial peptides from plant source and the catalytic domain of diphtheria toxin are shown.

S. No.	**AMP**	**Global Energy (kcal/mol)**	**Non Bond interactions**	**No. of H bond**
1.	JCPep7	-11.60	6	1
2.	Antimicrobial Peptide 1	-36.92	10	2
3.	Cr-ACP1	-12.67	4	0
4.	Sesquin	-19.31	6	2
5.	Alliumin	**-31.64**	14	**4**

The global energy of the docked complex of catalytic domain of diphtheria toxin with Antimicrobial peptide 1 is least. Considering the global energies, number of hydrogen bonds and the crucial residues of diphtheria toxin interacting with the antimicrobial peptide, the docked complex of catalytic domain of diphtheria toxin and Alliumin is considered best for further molecular dynamics studies.

4.3.3 Molecular dynamics simulation results

Molecular dynamics simulation was carried out using GROMACS. The 3D structure of ToxT, docked complex of catalytic domain of diphtheria toxin + Microcin C7 and docked complex of catalytic domain of diphtheria toxin + Alliumin were simulated for 10ns. The values of root mean square deviation (RMSD) and root mean square fluctuation (RMSF) for the above simulations were compared.

The total charge on DT, docked complex of DT + Microcin C7 and docked complex of DT + Alliumin was -7, -6 and -9 respectively. These charges were neutralized by adding 7, 6 and 9 sodium ions to DT, docked complex of DT + Microcin C7 and docked complex of DT + Alliumin respectively. On comparing the RMSD values of all the above three simulations (shown in FIGURE 4.46) it was seen that the minimum fluctuations were seen in the RMSD values of DT + Alliumin. High fluctuation is seen in the RMSD values of DT + Microcin C7 till around 6ns after that the values become stable. The values of RMSD for DT keeps on increasing till 6ns and afterwards becomes a bit stable but the fluctuations are more as compared to the RMSD values of the DT + Microcin C7. The values of RMSD for docked complex of DT + Alliumin increase from 0ns to 2.6ns, after that the values stabilize. The RMSD values for the docked complex of DT + Alliumin show least fluctuations and hence the docked complex of DT + Alliumin is the most stable complex among all the three structures.

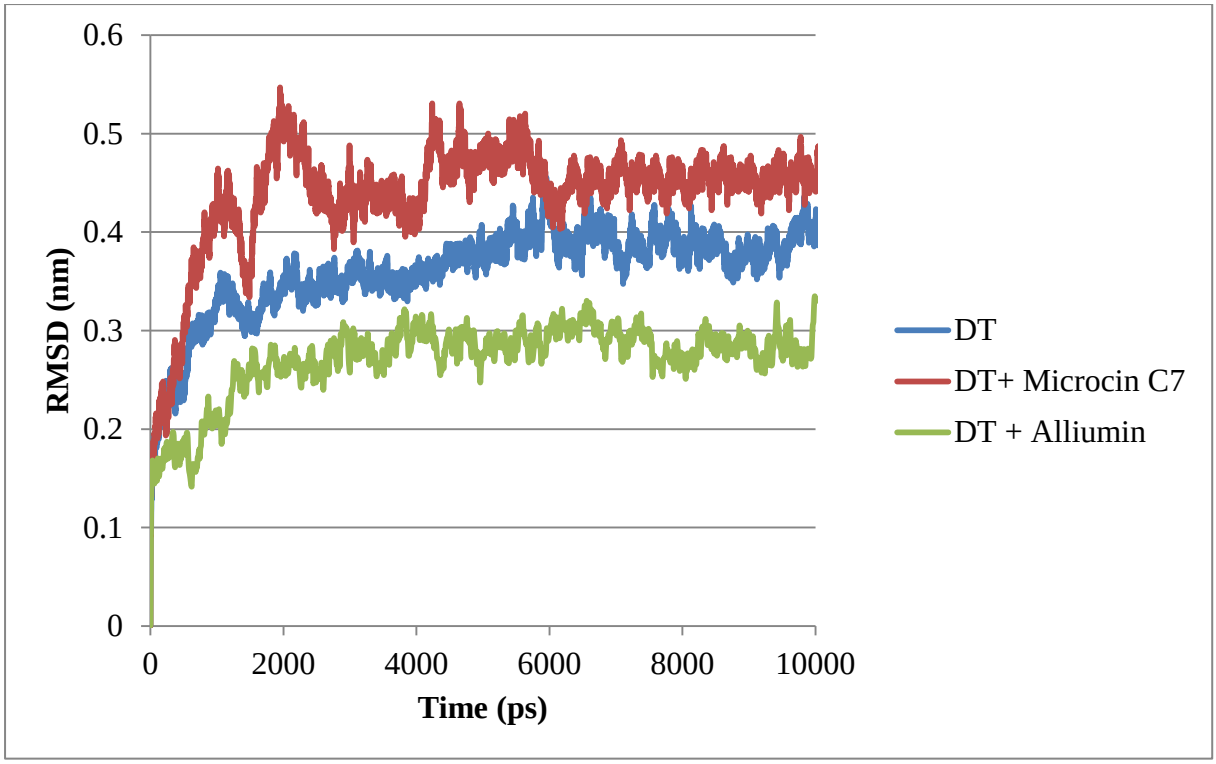

FIGURE 4.46: Comparative plot for the RMSD values of DT, docked complex of DT+Microcin C7 and docked complex of DT+Alliumin. The green line of RMSD plot of docked complex of DT and Alliumin shows the most stability.

On comparing the RMSF values of all the three simulations (shown in FIGURE 4.47) it is seen that minimum fluctuations are observed for the docked complex of DT + Alliumin. It is observed that the RMSF fluctuations for the interacting residues of catalytic domain of diphtheria toxin as well as the other crucial residues of the diphtheria toxin show least fluctuations for the docked complex of DT + Alliumin. Lesser the values of RMSF means more stability of the atoms. This reveals that the crucial residues atoms and interacting residues atoms are most stable at their position in the docked complex of DT and Alliumin.

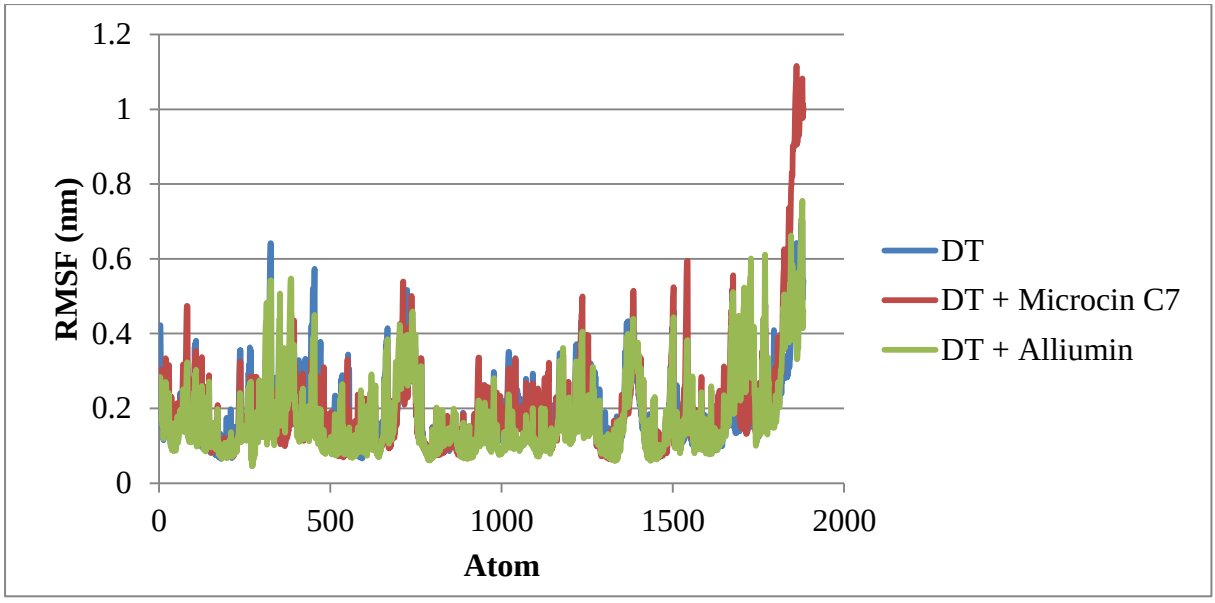

FIGURE 4.47: Comparative plot for the RMSF values of DT, docked complex of DT+Microcin C7 and docked complex of DT+Alliumin. The predicted structural stability of the complex of DT and Alliumin is maximum among these.

Comparison of the values of RMSD and RMSF of all the three simulations show that the docked complex of the catalytic domain of diphtheria toxin and Alliumin is most stable. Hence, we can conclude that the Alliumin is better drug candidate against diphtheria toxin as compared to Microcin C7.

The value of the radius of gyration of the catalytic domain of diphtheria toxin and the docked-complex were compared. (shown in FIGURE 4.48). The radius of gyration reveals about the compactness of the structure. It was observed that the fluctuations of the docked complex for the radius of gyration are less as compared to the fluctuations of the radius of gyration of the catalytic domain of diphtheria toxin. The range of radius of gyration for the catalytic domain of diphtheria toxin is more than the range of radius of gyration of the docked complex. Thus, the docked complex is more compact as compared to the catalytic domain of diphtheria toxin. Hence, the docked complex is more stable than the catalytic domain of diphtheria toxin.

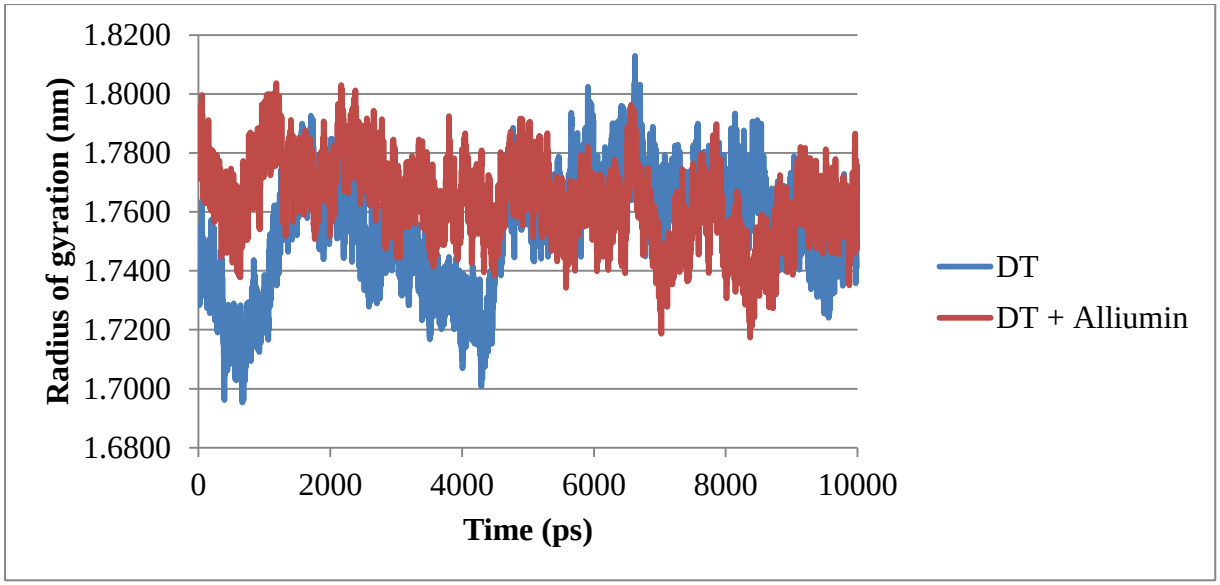

FIGURE 4.48: Comparative plot for the Radius of gyration values of DT and docked complex of DT+Alliumin. The predicted compactness of structure of docked complex of DT and Alliumin is more than that of DT.

The simulation was performed for 20 ns and the hydrogen bonds were calculated. The number of hydrogen bonds was calculated between the catalytic domain of diphtheria toxin and peptide (shown in FIGURE 4.49). The number of hydrogen bonds formed between DT and Alliumin throughout the simulation time ranged from 1 to 13. Maximum time the number

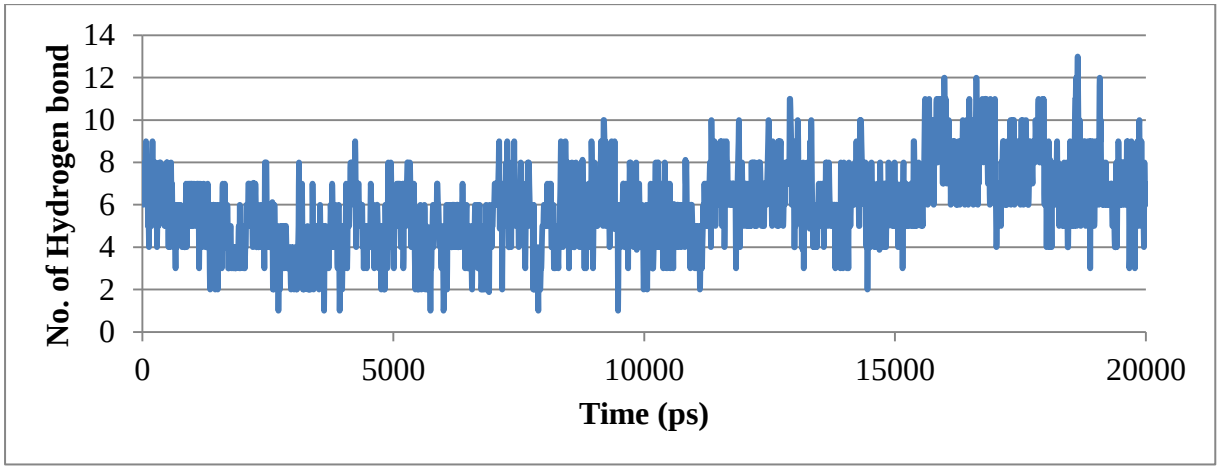

FIGURE 4.49: Number of hydrogen bonds formed between catalytic domain of diphtheria toxin and Alliumin throughout simulation of 20ns.

of hydrogen bonds ranged from 4 to 7. Thus, it was predicted that the hydrogen bond interaction between receptor and peptide continues as the simulation proceeds.

4.3.4 DISCUSSION

The 3D structures of all the ten short length antimicrobial peptides selected for our studies were docked with catalytic domain of diphtheria toxin. On comparing the docking results of antimicrobial peptides from microorganism sources it was observed that the least global energy was found to be that of Curvalicin-28c docked complex, i.e., -47.39 kcal/mol. Only one hydrogen bond was formed between Curvalicin-28c and catalytic domain of diphtheria toxin. None of the crucial residues of diphtheria toxin was involved in hydrogen bond formation with Curvalicin-28c. Microcin C7 docked complex has a global energy -43.23 kcal/mol. Microcin C7 forms three hydrogen bonds with catalytic domain of diphtheria toxin and one crucial residue of diphtheria toxin, i.e., Thr42 is involved in hydrogen bond formation. Hence, it was predicted that Microcin C7 gave a best docking result among the set of five antimicrobial peptides of plant source and was taken for further molecular dynamics studies.

Comparison of the docking results of the selected antimicrobial peptides from plant source showed that although the least global energy was of the docked complex of Antimicrobial peptide1 but the best docked complex was that of catalytic domain of diphtheria toxin and Alliumin. The global energy of the docked complex of Antimicrobial peptide 1 was -36.92 kcal/mol, the number of hydrogen bonds formed between Antimicrobial peptide 1 and diphtheria toxin were two and the crucial residues involved in hydrogen bond formation between Antimicrobial peptide 1 and diphtheria toxin was Lys24. The global energy of the docked complex of Alliumin was -31.64 kcal/mol, the number of hydrogen bonds formed between Alliumin and diphtheria toxin were four and the crucial residues involved in hydrogen bond formation between Alliumin and diphtheria toxin were Lys24, Gly44, Tyr54

and Tyr65. Hence, it was observed that Alliumin gave the best docking results with the catalytic domain of diphtheria toxin among all the five selected antimicrobial peptides and the docked complex was further considered for molecular dynamics studies.

The comparison of the RMSD results of the catalytic domain of diphtheria toxin alone, docked complex of DT + Microcin C7 and docked complex of DT + Alliumin showed the least fluctuations in the RMSD values for the docked complex of DT + Alliumin . Thus it was predicted that the docked complex of DT + Alliumin was most stable among all the three structures. The comparison of RMSF values of the all the structures showed that the atoms of the crucial residues of diphtheria toxin and the atoms of the residues of diphtheria toxin involved in interaction with the antimicrobial peptides showed least fluctuations at their position, which predicts the greater stability of the structure of the docked complex of catalytic domain of diphtheria toxin and Alliumin. Thus, it was predicted that Alliumin gave better interaction with catalytic domain of diphtheria toxin as compared with the Microcin C7. Alliumin was thus used for further analysis. On comparing the values of radius of gyration for catalytic domain of diphtheria toxin alone with the docked complex of DT + Alliumin it was seen that less fluctuation was seen in the values of radius of gyration for the docked complex of DT + Alliumin. Radius of gyration gives the compactness of the structure. The above observation showed that the structure of the docked complex of DT + Alliumin is more compact and thus more stable. The number of hydrogen bonds was analysed for 20 ns for the docked complex of DT + Alliumin. The number of hydrogen bonds ranged from 1 to 13 during the time of simulation. Thus, it was seen that hydrogen bonding is present throughout as the simulation proceeds.

4.4 Interaction of Alliumin with *Vibrio cholerae* transcription activator ToxT

4.4.1 Docking results

The best docking complex of interaction of ToxT with Alliumin shows (shown in FIGURE 4.50) protein-peptide interaction energy -28.58kcal/mol. Ser70 residue of ToxT forms hydrogen bonds with Lys4 and Cys5 residues of Alliumin. Thr253 residue of ToxT forms two hydrogen bonds with Lys10 residue of Alliumin. Asn23 residue of ToxT forms hydrogen bonds with Gly8 and Cys9 residues of Alliumin. Ile21 residue of ToxT forms alkyl interaction with Ala6 residue of Ala6 residue of Alliumin. Ile43 residue of ToxT forms Pi-alkyl interaction with Phe3 residue of Alliumin. Six hydrogen bonds are formed between ToxT and Alliumin. Thr253 is the crucial residue of ToxT which interacts with antimicrobial peptide Alliumin and forms hydrogen bonds with it.

Thus, it was observed that the antimicrobial peptide alliumin interacts significantly with transcription activator ToxT. This docked complex was further simulated for 20 ns.

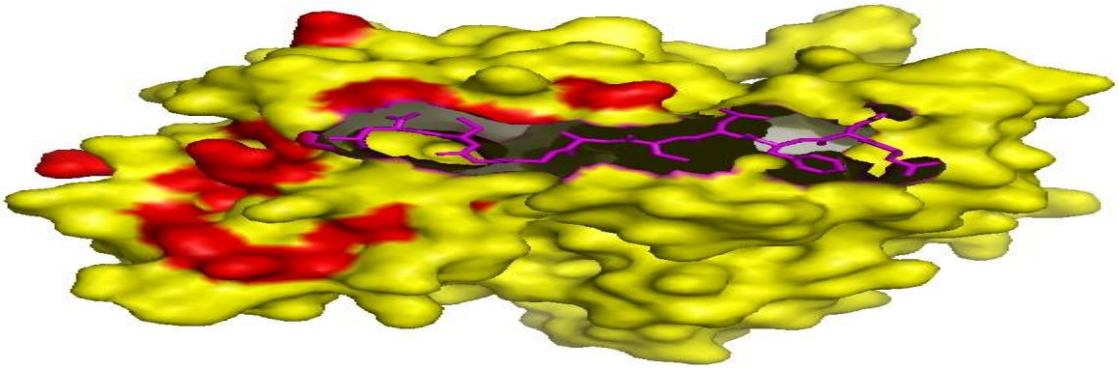

FIGURE 4.50: The figure shows the docked complex of ToxT and Alliumin. The yellow residues represent the residues of ToxT, red residues represent the crucial residues of ToxT and the magenta residues represent the residues of antimicrobial peptide Alliumin.

4.4.2 Molecular dynamics simulation results

Molecular dynamics simulation was carried out using GROMACS. The modelled 3D structure of ToxT and docked complex of ToxT-Alliumin were simulated for 20ns. The

values of root mean square deviation (RMSD), root mean square fluctuation (RMSF), hydrogen bond and radius of gyration (Rg) for the above simulations were compared.

The total charge on ToxT and docked complex of ToxT+Alliumin was 5 and 3 respectively. These charges were neutralized by adding 5 and3 chloride ions to ToxT and docked complex of ToxT+Alliumin respectively. On comparing the values of RMSD (shown in FIGURE 4.51) for both the simulations it was observed that the fluctuations were high for ToxT alone as compared to the docked complex of ToxT+Alliumin. Till 4ns the RMSD values for ToxT are little less than the RMSD values for ToxT+Alliumin complex. Till nearly 5.5ns the RMSD values for ToxT are nearly the same as the RMSD values for ToxT + Alliumin complex. After 5.5ns the RMSD values of ToxT is more than the RMSD values for ToxT +Allliumin dockd complex. The RMSD values for ToxT keep on increasing nearly till 8.2ns and then fluctuations nearly stabilize around the value 0.35 nm. While the RMSD values for ToxT + Alliumin complex increase till 1.5 ns and then these values nearly stabilize around 0.3 nm. The RMSD values of ToxT show greater fluctuations in the stable region as compared to the RMSD values of ToxT + Alliumin complex in the stable region. Thus, it is predicted that ToxT becomes more stable when bound to antimicrobial peptide Alliumin as compared to its native structure.

On comparing the values of RMSF (shown in FIGURE 4.52) for both the simulations it was observed that for most residues the values of RMSF for ToxT is more than the values of RMSF for the complex ToxT + Alliumin. Only for some residues of amino acids Gln8-Val11, Ile43-Ser50 and Asn122- Asn132 the RMSF values of ToxT are little less than the RMSF values of complex ToxT + Alliumin. These specified amino acids do not belong to the crucial residues of ToxT, also these residues do not interact with Alliumin. The RMSF values for ToxT + Alliumin complex are less for the crucial residues of ToxT and also the

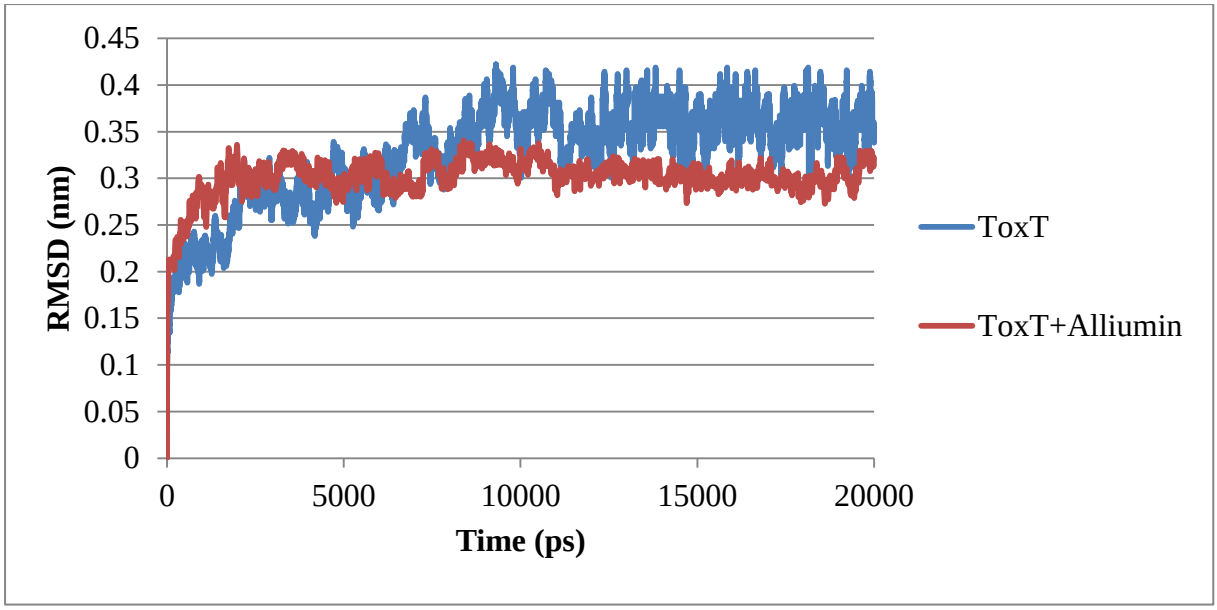

FIGURE 4.51: Comparative plot for the RMSD values of ToxT and docked complex of ToxT+Alliumin. The red line of RMSD plot of docked complex of ToxT and Alliumin shows the most stability.

interacting residues of ToxT with Alliumin. This predicts that these residues show less fluctuation in the complex as compared to the native ToxT and thus show more stability. Thus, the crucial and interacting residues show more stability after ToxT binds with antimicrobial peptide alliumin.

Observation of the intermolecular hydrogen bonds (shown in FIGURE 4.53) for the docked complex of ToxT + Alliumin shows that throughout the 20ns molecular dynamics simulation the number of inter molecular hydrogen bond formed ToxT and Alliumin range between 1 to 11. This analysis shows that the hydrogen bond interaction between ToxT and Alliumin continues throughout the simulation.

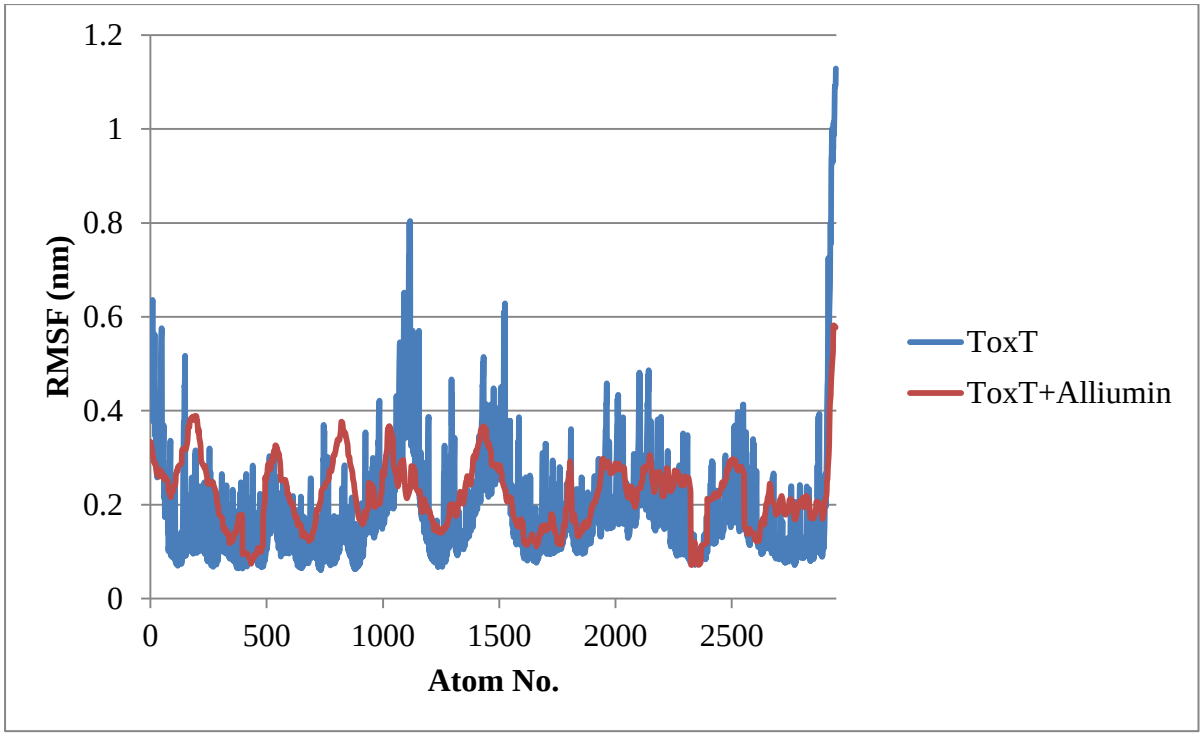

FIGURE 4.52: Comparative plot for the RMSF values of ToxT and docked complex of ToxT+Alliumin The predicted structural stability of the complex of ToxT and Alliumin, shown in red, is maximum among these.

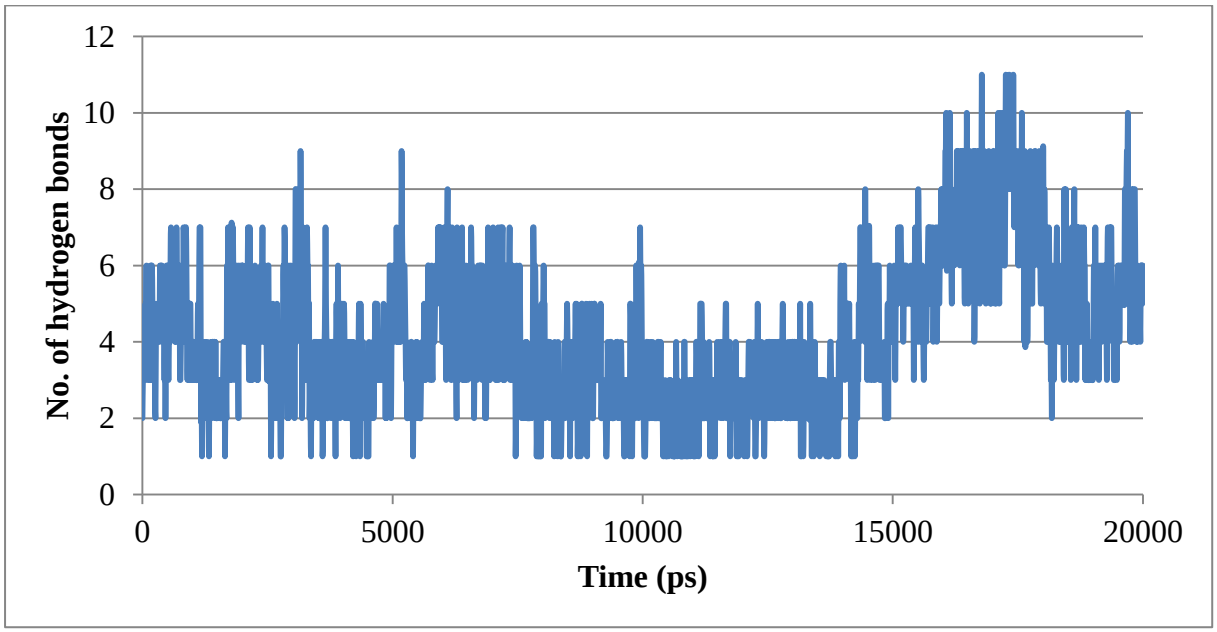

FIGURE 4.53: Plot for the intermolecular hydrogen bond values for docked complex of ToxT+Alliumin

On comparing the values of Radius of gyration (shown in FIGURE 4.54) for both the simulations it was observed that the fluctuations in the radius of gyration values for ToxT is higher than the fluctuations in the radius of gyration values for complex ToxT + Alliumin. The range of minimum and maximum values for radius of gyration for ToxT is more than the range for values of radius of gyration for complex ToxT + Alliumin. The less fluctuation in the radius of gyration values for complex of ToxT + Alliumin predicts that the structure of complex is more compact than the structure of native ToxT.

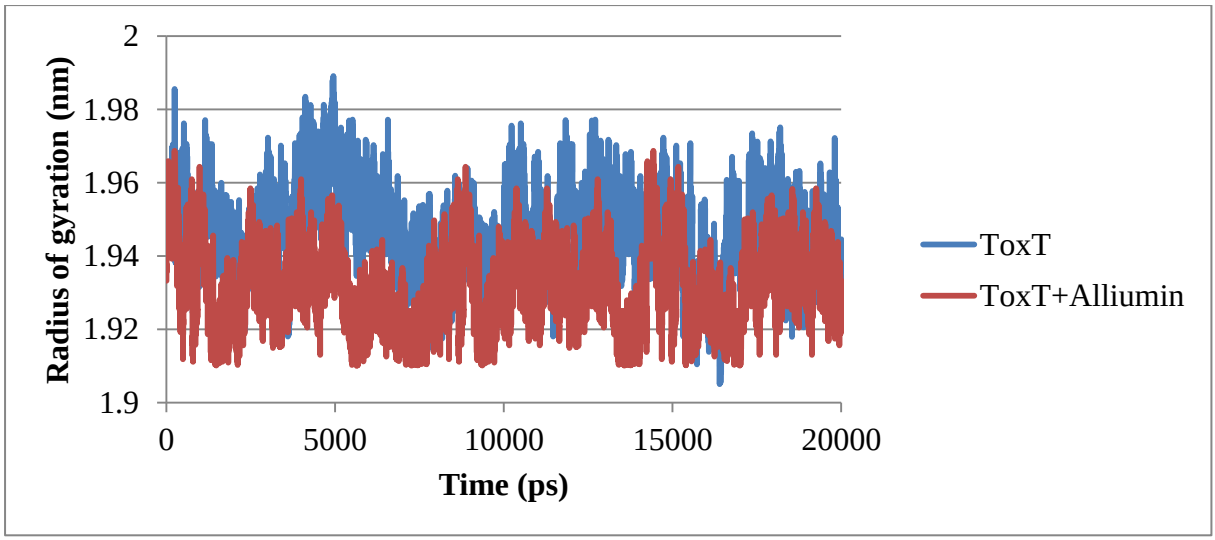

FIGURE 4.54: Comparative plot for the Radius of gyration values of ToxT and docked complex of ToxT+Alliumin . The predicted compactness of structure of docked complex of ToxT and Alliumin, shown in red, is more than that of ToxT.

4.4.3 DISCUSSION

The best docked complex formed between ToxT and Alliumin had protein-peptide interaction energy -28.58 kcal/mol. Six intermolecular hydrogen bonds were formed. One crucial residue of ToxT Thr253 was involved in interaction with antimicrobial peptide Alliumin. Further the RMSD results showed that the fluctuations decreased in the docked complex as compared to the native structure of ToxT. Thus increasing the stability of ToxT after it binds to the

antimicrobial peptide Alliumin. The RMSF values comparison showed that the fluctuations of the crucial residues of ToxT and those residues involved in interaction with Alliumin decreased after ToxT binds with Alliumin. Thus making them more stable about their mean position and increasing the stability of the complex. The analysis of the hydrogen bonds throughout the simulation time showed that the intermolecular hydrogen bonds are present throughout the simulation time. These show that significant intermolecular interactions are present between ToxT and Alliumin throughout simulation. The radius of gyration values comparison showed that the there is greater fluctuations during a wide range of values for native ToxT structure as compared to the docked complex. These predict that the docked complex is more complex and stable than the native structure of ToxT.

4.5 Interaction of Alliumin with New Delhi Metallo-beta-lactamase 1

4.5.1 Modelled structure of NDM-1

The 3D structure of NDM-1 in 3Q6X had missing residues in it. Thus the structure of NDM-1 had to be modelled using I-TASSER. I-TASSER returned five models as output. Model-1 has C-score 0.93 and estimated TM-score was 0.60±0.14 and was selected for further studies based upon C-score, TM-score and RMSD. Now the modelled structure was a 3D structure with all the amino acids complete in the chain.

The modelled structure of NDM-1 using I-TASSER webserver is shown in FIGURE 4.55.

4.5.2 Docking results

The best docking complex of interaction of NDM-1 with Alliumin shows (shown in FIGURE 4.56) protein-peptide interaction energy -22.80 kcal/mol. Lys216 residue of NDM-1 is involved in electrostatic interaction with Asp2 residue of Alliumin. Gln123 residue of NDM-

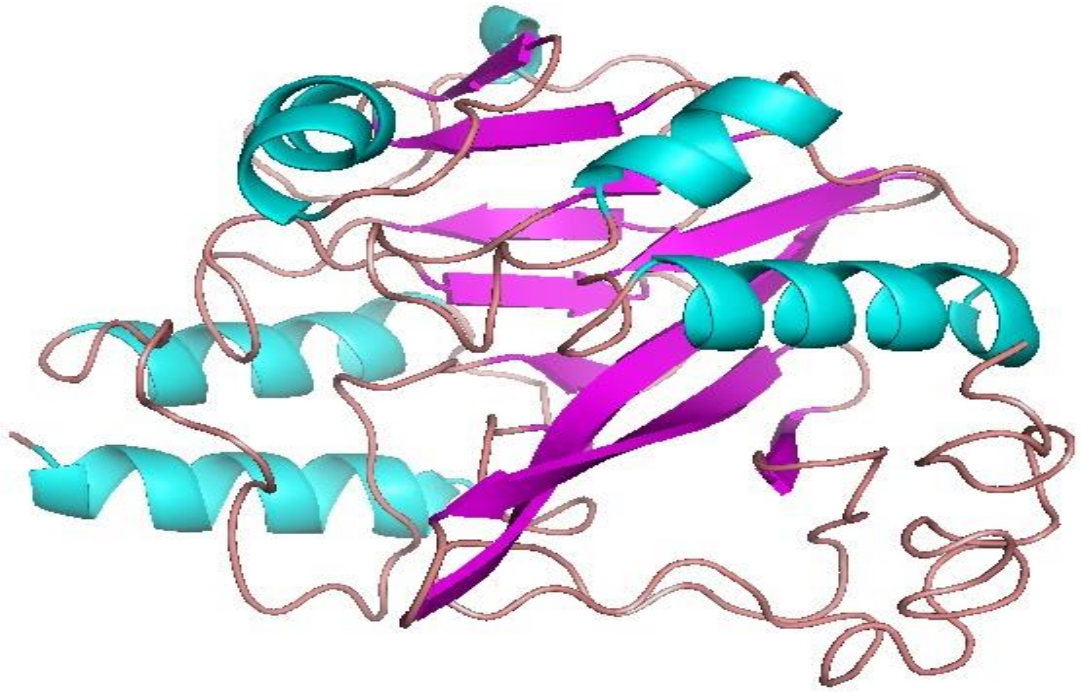

FIGURE 4.55: Modelled structure of NDM-1.

1 forms hydrogen bonds with GLy7 and Cys9 residues of Alliumin. Ser217 residue of NDM-1 forms two hydrogen bonds with Phe3 residue of Alliumin. Asn220 residue of NDM-1 forms hydrogen bond with Leu4 residue of Alliumin. Gly219 residue of NDM-1 forms carbon hydrogen bond with Phe3 residue of Alliumin. Asp124 residue of NDM-1 form carbon hydrogen bond with Gly7 residue of Alliumin. His250 residue of NDM-1 forms Pi-Sulfur interaction with Cys5 residue of Alliumin. Met67 forms alkyl interactions with Leu4, ALa6 and Cys9 residues of Alliumin. Pro68 and Val73 residues of NDM-1 form alkyl interactions with Cys9 and Ala6 residues respectively of Alliumin. Phe70, Trp93, His189 and Ala215 residues of NDM-1 form Pi-Alkyl interactions with Leu4, Ala6, Cys5 and Phe3 residues respectively of Alliumin. The crucial residues His250, Lys216, Gln123, Asp124, His189, Asn220, Met67, Pro68 and Val73 of NDM-1 are involved in interaction with Alliumin.

Thus, it was observed that the antimicrobial peptide alliumin interacts significantly with NDM-1. This docked complex was further simulated for 20 ns.

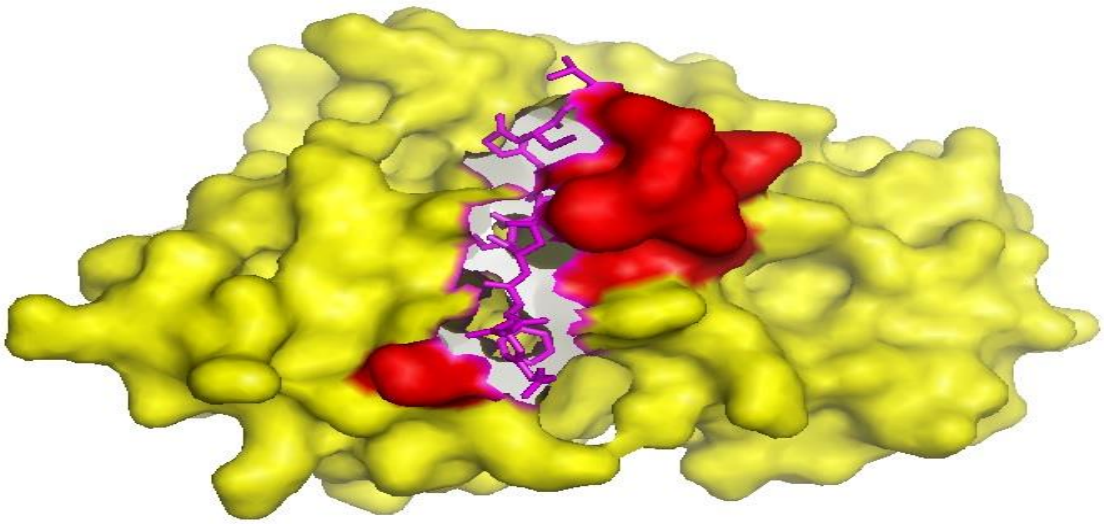

FIGURE 4.56: The figure shows the docked complex of NDM-1 and Alliumin. The yellow residues represent the residues of NDM-1, red residues represent the crucial residues of NDM-1 and the magenta residues represent the residues of antimicrobial peptide Alliumin.

4.5.3 Molecular dynamics simulation results

Molecular dynamics simulation was carried out using GROMACS. The modelled 3D structure of NDM-1 and docked complex of NDM-1-Alliumin were simulated for 20ns. The values of root mean square deviation (RMSD), root mean square fluctuation (RMSF), hydrogen bond and radius of gyration (Rg) for the above simulations were compared.

On comparing the values of RMSD (shown in FIGURE 4.57) for both the simulations it was observed that the fluctuations were high for NDM-1 alone as compared to the docked complex of NDM-1+Alliumin. Till nearly 0.2ns the RMSD values for NDM-1 are nearly the same as the RMSD values for NDM-1 + Alliumin complex. After 0.2ns the RMSD values of

NDM-1 is more than the RMSD values for NDM-1 +Allliumin dockd complex. The RMSD values for NDM-1 keep on increasing nearly till 8ns and then fluctuations nearly stabilize around the value 0.35 nm. While the RMSD values for NDM-1 + Alliumin complex increase till 5.2 ns and then these values nearly stabilize around 0.3 nm. The RMSD values of NDM-1 show greater fluctuations in the stable region as compared to the RMSD values of NDM-1 + Alliumin complex in the stable region. Thus, it is predicted that NDM-1 becomes more stable when bound to antimicrobial peptide Alliumin as compared to its native structure.

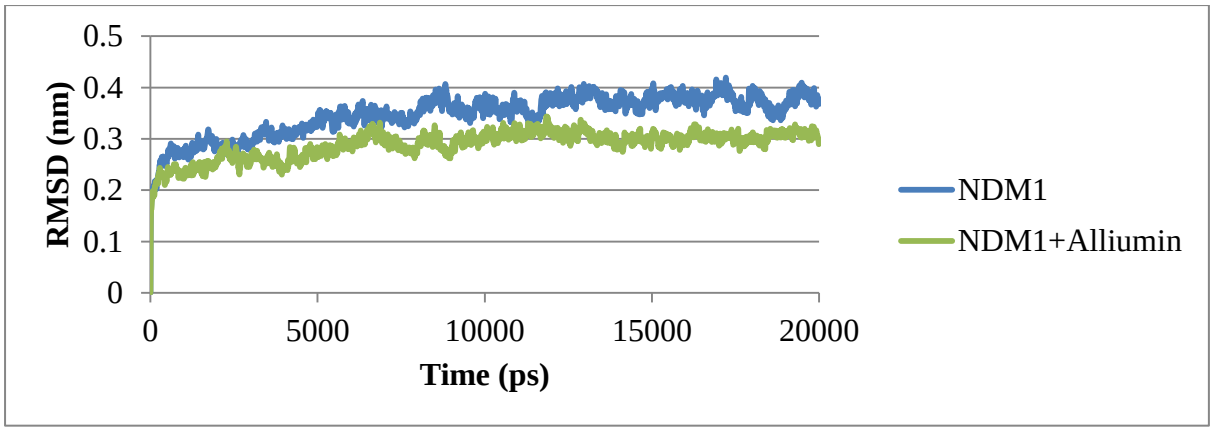

FIGURE 4.57: Comparative plot for the RMSD values of NDM-1 and docked complex of NDM-1+Alliumin. The green line of RMSD plot of docked complex of NDM-1 and Alliumin shows the most stability.

On comparing the values of RMSF (shown in FIGURE 4.58) for both the simulations it was observed that for most residues the values of RMSF for NDM-1 is more than the values of RMSF for the complex NDM-1 + Alliumin. Only for some residues of amino acids 1-14, 22, 40-60 and 200-214 the RMSF values of NDM-1 are little less than the RMSF values of complex NDM-1 + Alliumin. These specified amino acids do not belong to the crucial residues of NDM-1, also these residues do not interact with Alliumin. The RMSF values for NDM-1 + Alliumin complex are less for the crucial residues of NDM-1 and also the interacting residues of NDM-1 with Alliumin. This predicts that these residues show less

fluctuation in the complex as compared to the native NDM-1 and thus show more stability. Thus, the crucial and interacting residues show more stability after NDM-1 binds with antimicrobial peptide alliumin.

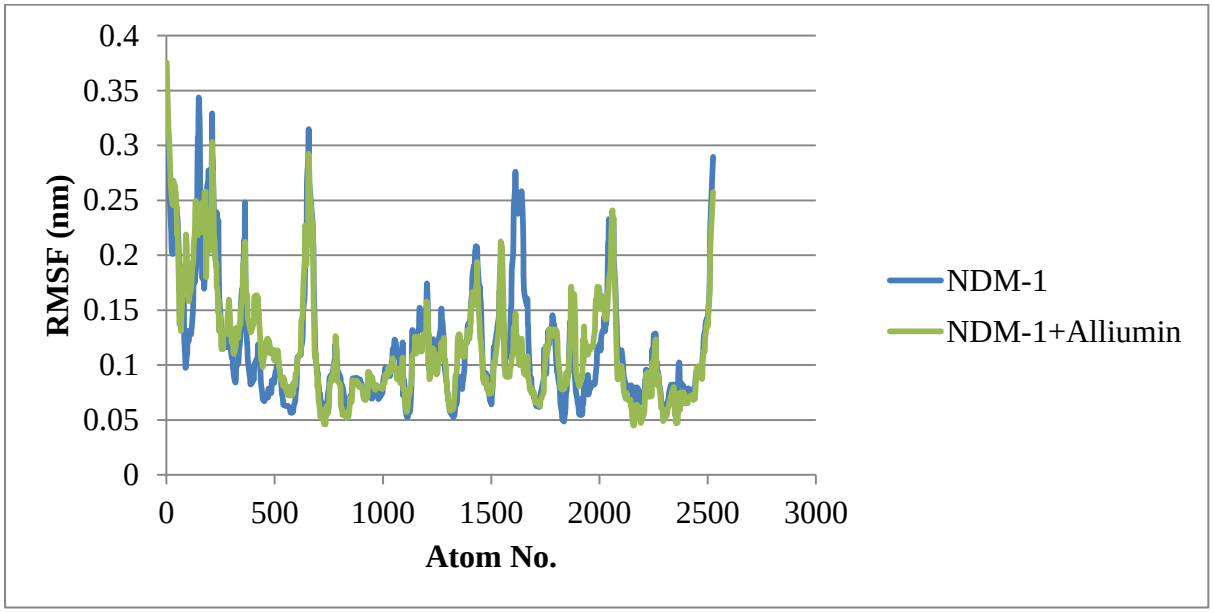

FIGURE 4.58: Comparative plot for the RMSF values of NDM-1 and docked complex of NDM-1+Alliumin. The predicted structural stability of the complex of NDM-1 and Alliumin, shown in green, is maximum among these.

Observation of the intermolecular hydrogen bonds (shown in FIGURE 4.59) for the docked complex of NDM-1 + Alliumin shows that throughout the 20ns molecular dynamics simulation the number of inter molecular hydrogen bond formed NDM-1 and Alliumin range between 1 to 11. This analysis shows that the hydrogen bond interaction between NDM-1 and Alliumin continues throughout the simulation.

On comparing the values of Radius of gyration (shown in FIGURE 4.60) for both the simulations it was observed that the fluctuations in the radius of gyration values for NDM-1 is higher than the fluctuations in the radius of gyration values for complex NDM-1 +

Alliumin. The range of minimum and maximum values for radius of gyration for NDM-1 is more than the range for values of radius of gyration for complex NDM-1 + Alliumin. The

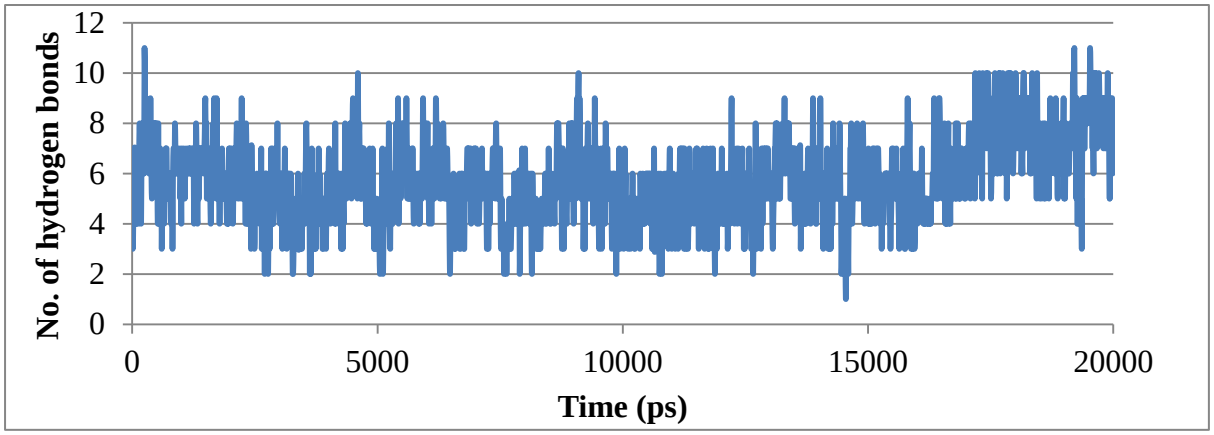

FIGURE 4.59: Plot for the intermolecular hydrogen bond values for docked complex of NDM-1+Alliumin.

less fluctuation in the radius of gyration values for complex of NDM-1 + Alliumin predicts that the structure of complex is more compact than the structure of native NDM-1.

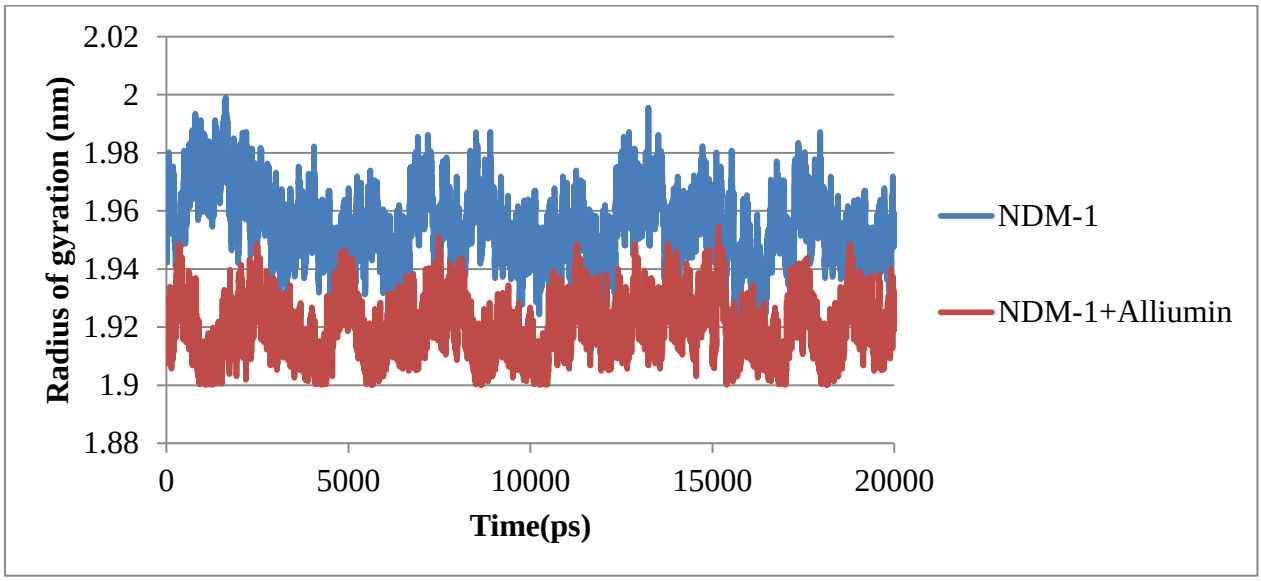

FIGURE 4.60: Comparative plot for the Radius of gyration values of NDM-1 and docked complex of NDM-1+Alliumin. The predicted compactness of structure of docked complex of NDM-1 and Alliumin, shown in red, is more than that of NDM-1.

4.5.4 DISCUSSION

The best docked complex formed between NDM-1 and Alliumin had protein-peptide interaction energy -22.8 kcal/mol. Four intermolecular hydrogen bonds were formed. One crucial residue of NDM-1 His250, Lys216, Gln123, Asp124, His189, Asn220, Met67, Pro68 and Val73 were involved in interaction with antimicrobial peptide Alliumin. Further the RMSD results showed that the fluctuations decreased in the docked complex as compared to the native structure of NDM-1. Thus increasing the stability of NDM-1 after it binds to the antimicrobial peptide Alliumin. The RMSF values comparison showed that the fluctuations of the crucial residues of NDM-1 and those residues involved in interaction with Alliumin decreased after NDM-1 binds with Alliumin. Thus making them more stable about their mean position and increasing the stability of the complex. The analysis of the hydrogen bonds throughout the simulation time showed that the intermolecular hydrogen bonds are present throughout the simulation time. These show that significant intermolecular interactions are present between NDM-1 and Alliumin throughout simulation. The radius of gyration values comparison showed that the there is greater fluctuations during a wide range of values for native NDM-1 structure as compared to the docked complex. These predict that the docked complex is more complex and stable than the native structure of NDM-1.

4.6 Synthesis of Alliumin and studies to check its antimicrobial properties

4.6.1 In silico characterization of Alliumin

In silico characterization using ProtParam, ToxinPred and HemoPred gave the results shown in TABLE 4.6.

TABLE 4.6: Properties of Alliumin characterized in silico

Sequence	DDFLCAGGCL

Molecular weight	1013.1 Da
Theoretical pI	3.56
Charge	-2
Formula	$C_{42}H_{64}N_{10}O_{15}S_2$
Total no. of atoms	133
Toxicity	Non-Toxic
Hemolytic/NonHemolytic	Non-Hemolytic

4.6.2 Synthesized Peptide

The USV (P) Ltd synthesized the Alliumin using the sequence sent to them. Code number given to the product was CPS- 2132.

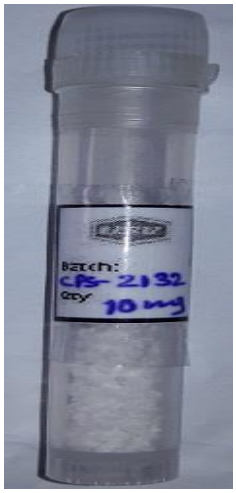

FIGURE 4.61: The synthesized peptide Alliumin procured from USV (P) Ltd Custom Peptide

4.6.3 Mass spectroscopy of synthesized peptide

The MS data of synthesized Alliumin sent by USV (P) Ltd (shown in FIGURE 4.62) shows the highest peak at 1013.6 Da which is nearly equal to the Molecular weight of Alliumin calculated in silico using ProtParam Tool.

FIGURE 4.62: MS data of synthesized Alliumin sent by USV (P) Ltd.

TABLE 4.7: Analytical Data Sheet of Synthesized Alliumin

Product	Linear Peptide
Code Number	CPS 2132
Quantity	10mg
Physical Appearance	White to Off-White Solid
Molecular Weight	1013.5 Da
HPLC Purity	>95%
Mass Obtained	1013.6 Da

4.6.4 ANTIBACTERIAL ASSAY

The antibacterial assay showed that the synthesized peptide Alliumin showed antibacterial activity both towards gram positive *Staphylococcus aureus* and gram negative *Escherichia coli.* The zone of inhibition is seen in the plate (shown in FIGURE 4.63). The antibacterial activity of synthesized Alliumin towards *Staphylococcus aureus* in more as compared to *Escherichia coli* as shown by the Zone of inhibition in TABLE 4.8.

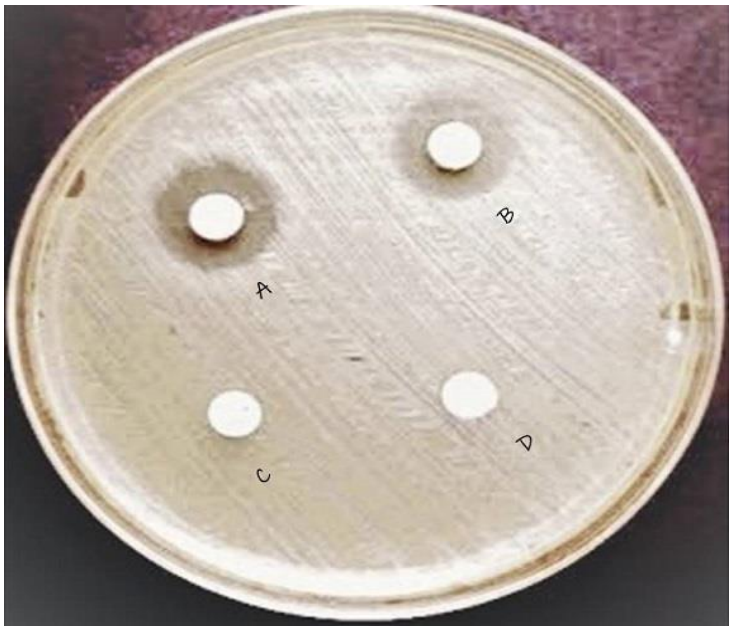

FIGURE 4.63: Zone of inhibition of Synthesied Alliumin against *Staphylococcus aureus (A)* and *Escherichia coli (B).* The controls C and D show do not show any zones of inhibition.

TABLE 4.8: Zone of inhibition of synthesized Alliumin against *E.coli* and *S. aureus*

Microorganism	**Zone of inhibition (mm)**
Escherichia coli	10.8
Staphylococcus aureus	11.3

4.6.5 DISCUSSION

The in silico characterization of sequence of Alliumin through ProtParam Tools predicted the molecular weight 1013.1 Da, charge of peptide to be -2 and Theoretical pI to 3.56. Alliumin is an anionic antimicrobial peptide having molecular weight nearly 1kDa. The Toxicity and Hemolytic activity predicted in silico using ToxinPred and HemoPred respectively predicted Alliumin to be non-Toxic and non-hemolyic. 10m Alliumin was procured from USV (P) Ltd, having purity >95%. The MS Data for synthesized Alliumin gave a high peak at 1013.6 Da. This value of mass equalled with the value of molecular weight predicted in silico. The antibacterial assay against *Staphylococcus aureus* and *Escherichia coli* showed more activity of synthesized Alliumin against *Staphylococcus aureus*. Zones of inhibition against *E.coli* and *S. aureus* with synthesized Alliumin were 10.8 mm and 11.3 mm respectively.